Pergamon

PII: S0191-8141(97)00076-X

Journal of Structural Geology, Vol. 19, No. 12, pp. 1495 to 1520, 1997
© 1997 Elsevier Science Ltd
All rights reserved. Printed in Great Britain
0191-8141/97 $17.00 + 0.00

Evidence for dominant grain-boundary sliding deformation in greenschist- and amphibolite-grade polymineralic ultramylonites from the Redbank Deformed Zone, Central Australia

TIMON F. FLIERVOET,* STANLEY H. WHITE and MARTYN R. DRURY

Geodynamics Research Institute, Faculty of Earth Sciences, Utrecht University, Utrecht, The Netherlands

(*Received* 7 *April* 1997; *accepted in revised form* 15 *September* 1997)

Abstract—Microstructural and textural investigations by scanning (SEM) and transmission electron microscopy (TEM) techniques have been performed on samples taken across two quartzo-feldspathic mylonite zones from the Redbank Deformed Zone, Central Australia. One has been deformed at greenschist-facies (GS), the second at amphibolite-facies (Am), conditions. With increasing strain the rock type changes from protomylonite to mylonite to ultramylonite. The protomylonites and mylonites consist of alternating quartz and polymineralic quartz–feldspar bands. At the highest strains a homogeneous, fine-grained polymineralic ultramylonite occurs. Shear-zone geometry and microscale structures indicate that these ultramylonites experienced higher strains and were weaker than the encapsulating protomylonites and mylonites. TEM and SEM studies of the ultramylonites reveal a rectangular to square grain shape, a continuous alignment of grain and interphase boundaries across several grain diameters, a grain size (GS 0.5 μm; Am 5–11 μm) less than the equilibrium subgrain size, and open and void-containing grain and interphase boundaries. Analysis of local textures by electron back-scatter diffraction (EBSD) in the SEM showed a very weak crystallographic preferred orientation (CPO) for the quartz. The grain misorientation relationships are not consistent, with dislocation creep being the dominant deformation mechanism. All structures are of the type expected if grain-boundary sliding processes had contributed significantly to the deformation. Consequently, the deformation of such quartzo-feldspathic rocks, and by implication the rheology of the Redbank Deformed Zone, must have been controlled by the mechanical properties of these fine-grained polymineralic ultramylonites, deforming by grain-boundary sliding processes. This is in contrast to the pure quartz bands which deformed by dislocation-creep mechanisms and were less important in the rheology of the Redbank Deformed Zone. © 1997 Elsevier Science Ltd.

INTRODUCTION

In quartzo-feldspathic rocks deformed under middle- to upper-crustal conditions, shear deformation often results in a well-defined compositional banding of alternating quartzitic- and feldspathic ($\pm$phyllosilicate)-rich layers. These layers anastomose around less deformed feldspar augen (Wakefield, 1977; Behrmann and Mainprice, 1987). Within the quartz bands, dislocation creep has been inferred to be the dominant deformation mechanism (e.g. White, 1976, 1977; Watts and Williams, 1979; Lloyd and Knipe, 1992; Fliervoet and White, 1995). It is therefore generally assumed that the plastic flow strength of the crust under these conditions is controlled by wet quartzite deforming by dislocation-creep processes (e.g. White and Bretan, 1985; White *et al.*, 1986; Ord and Hobbs, 1989; Rutter and Brodie, 1991). The two major assumptions, as stated in White and Bretan (1985), are that: (i) quartz is forming a load-bearing framework; and (ii) that deformation is *not* partitioned into shear zones. The latter assumption raises the question—what happens when deformation is preferentially concentrated into major shear zones, especially when these become the loci for repeated deformation events due to reactivation? In such cases, these mechanically weak zones can have a significant control on crustal rheology.

With increasing strain, the microstructure of the mylonitic rocks changes from protomylonitic (0–50% matrix) to mylonitic (50–90% matrix) and eventually to ultramylonitic (90–100% matrix) (classification after Sibson, 1977). In the geological literature the term mylonite is commonly used in two ways. It can either refer to the entire zone of deformation or to a rock type having 50–90% matrix (Sibson, 1977; Passchier and Trouw, 1996). In the present paper, to avoid any confusion, we refer to a deformed rock having 50–90% matrix as a 'mylonite' and to the entire zone (irrespective of the mylonitic type) as a 'mylonite zone'. Within ultramylonites, the compositional layering generally vanishes and is replaced by a more homogeneous, fine-grained mixture made up of quartz $\pm$ K-feldspar $\pm$ plagioclase $\pm$ mica $\pm$ epidote in which the micas define the foliation (Wakefield, 1977; Knipe and Wintsch, 1985; Gilotti, 1992; Stünitz and Fitz Gerald, 1993). The actual mineralogy of this mixture depends on the metamorphic conditions during deformation.

Establishing the deformation mechanisms within such polyphase ultramylonites is essential to the understanding of the rheological behaviour of shear zones. However, usually the highly strained ultramylonites are characterized by a very fine grain size (< 10 μm) which generally hinders 'standard' microstructural and textural (CPO)

* Author to whom correspondence should be addressed at: Philips Electron Optics, Eindhoven, The Netherlands.

analyses. Detailed microstructural and (micro)textural studies by means of scanning (SEM) and transmission electron microscopy (TEM) are needed on these polymineralic ultramylonites to ascertain: (i) the deformation mechanisms within them; and (ii) whether quartz still provides the load-bearing framework, i.e. controls the rheology. Only then can the mechanical properties of deep crustal shear zones within quartzo-feldspathic rocks and their control on crustal rheology be established. A number of studies on such highly strained, polyphase ultramylonites indicate that their deformation is not controlled by wet quartzite deforming by dislocation-creep processes, but by a grain-size-sensitive creep mechanism during which grain-boundary sliding creep processes play a major role (e.g. Allison *et al.*, 1979; Behrmann and Mainprice, 1987; Stünitz and Fitz Gerald, 1993).

We have studied the microstructures and microtextures (CPO) of ultramylonites formed at middle- to upper-crustal levels from a major shear, the Redbank Deformed Zone of Central Australia, using light microscopy and both SEM and TEM techniques. The zone is known to be a transcrustal structure with a long history of multiple reactivation since its initiation (Goleby *et al.*, 1989; Shaw and Black, 1991). The shear zone exhibits zones of very fine-grained polymineralic ultramylonites encapsulated within coarser-grained (proto)mylonites. It contains mylonite zones of different metamorphic grade, which are thought to represent different crustal levels and which have been brought together during uplift. We will concentrate on the amphibolite-grade ultramylonites, with comparative studies on the greenschist-facies ultramylonites. The reason for this is that the coarser grain size of the former allowed both SEM and TEM analyses, whereas the very fine grain size of the latter precluded SEM work. Quartz (micro)textural analyses using SEM and TEM were only successful on the amphibolite-facies samples, as is discussed below. Data regarding the deformation mechanisms that allowed these ultrafine-grained polyphase ultramylonites to be weak under middle- to upper-crustal conditions are presented, and estimations of the relative partitioning of the strain between the mylonitic and ultramylonitic parts of the shear zones are given. We go on to compare these deformation mechanisms with those in discontinuous monomineralic bands of ultrafine quartz (cf. Fliervoet and White, 1995).

GEOLOGICAL SETTING AND FIELD DESCRIPTIONS

The samples studied were taken across two mylonite zones from the Redbank Deformed Zone (RBDZ) near Alice Springs, Central Australia (Fig. 1). This is a major thrust boundary (> 400 km long) separating a region of granulite-facies rocks in the north from greenschist- to amphibolite-facies rocks in the south (Shaw and Black, 1991; Black and Shaw, 1992). Seismic reflection profiles show that the RBDZ dissects the entire continental crust and extends into the upper mantle (Goleby *et al.*, 1989). The RBDZ itself is a 20 km wide complicated zone consisting of anastomosing mylonite zones (10–250 m wide) in a protomylonite matrix. The mylonite zones have in turn anastomosing zones of very fine-grained ultramylonites (typically from a few centimetres to a few tens of metres wide) amidst the coarser-grained mylonites. Two types of mylonitic shear zones have been recognized in the Redbank Deformed Zone (Shaw and Black, 1991): the first contains amphibolite-facies mineral

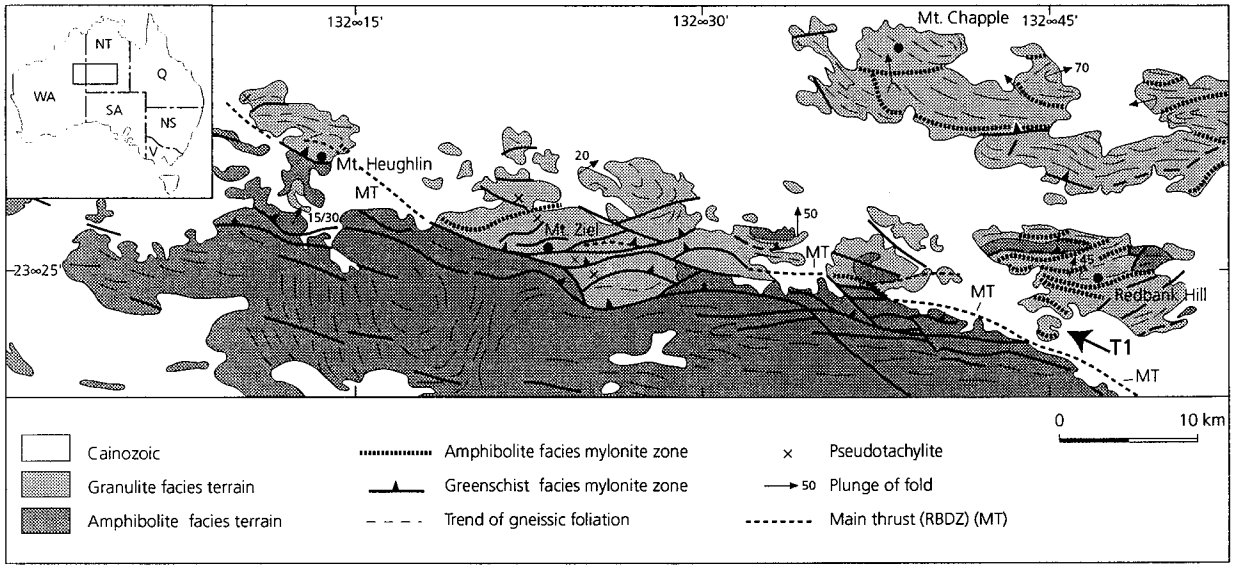

Fig. 1. Schematic map showing the distribution of amphibolite- and greenschist-facies ultramylonite zones in the Redbank Deformed Zone (after Shaw and Black, 1991). Position T1 indicates the amphibolite-facies mylonite zone sampling locality.

assemblages (550–650°C) and have been dated at ages between 1400 and 1500 Ma; the second contains greenschist-facies mineral assemblages (350–450°C) and have been dated at ages between 300 and 400 Ma. Although the two types of mylonite zones have quite different ages, they developed from similar country rocks. Therefore, the differences in metamorphic grade are thought to represent deformation at different crustal levels.

The amphibolite-facies mylonite zone sampled is *ca* 250 m wide and contains a 40–50 m wide dark ultramylonite in its centre; the zone is located south of Redbank Hill (grid reference: 7207800 N and 359500 E; Fig. 1) in an area previously studied by Marjoribanks and Black (1974) and Shaw and Black (1991). The greenschist-facies mylonite zone studied is a broad shear zone 200 m wide in the southeastern part of the New Well area (grid reference: 7389500 N and 356600 E) previously studied by Obee and White (1985, 1986). This broad zone contains several smaller-scale (2 m wide) mylonite zones from which samples have been taken (Obee and White, 1985, fig. 4).

Both the amphibolite- and greenschist-facies mylonite zones are marked by a moderately to steeply N-dipping mylonitic foliation (40–70°) and have a down-dip stretching lineation defined by elongate grains and aggregates of K-feldspar, plagioclase and quartz. Asymmetric porphyroclast systems, asymmetric folds and shear bands have been used as shear-sense indicators (cf. White *et al.*, 1986; Passchier and Trouw, 1996) and these consistently show a reverse sense of movement for both mylonite zones. The country rock surrounding the two studied mylonite zones is similar and consists of weakly foliated granitic gneiss with large feldspar augen (Fig. 2a).

In both of the selected mylonite zones, the matrix grain size decreases towards the centre of the individual shear zone. The feldspar clasts also decrease in size and form augen. The decrease in both matrix and augen grain size is thought to reflect an increase in deformation intensity. There is a corresponding increase in the amount of matrix to define a protomylonite–mylonite–ultramylonite sequence into the centre of the zones. In

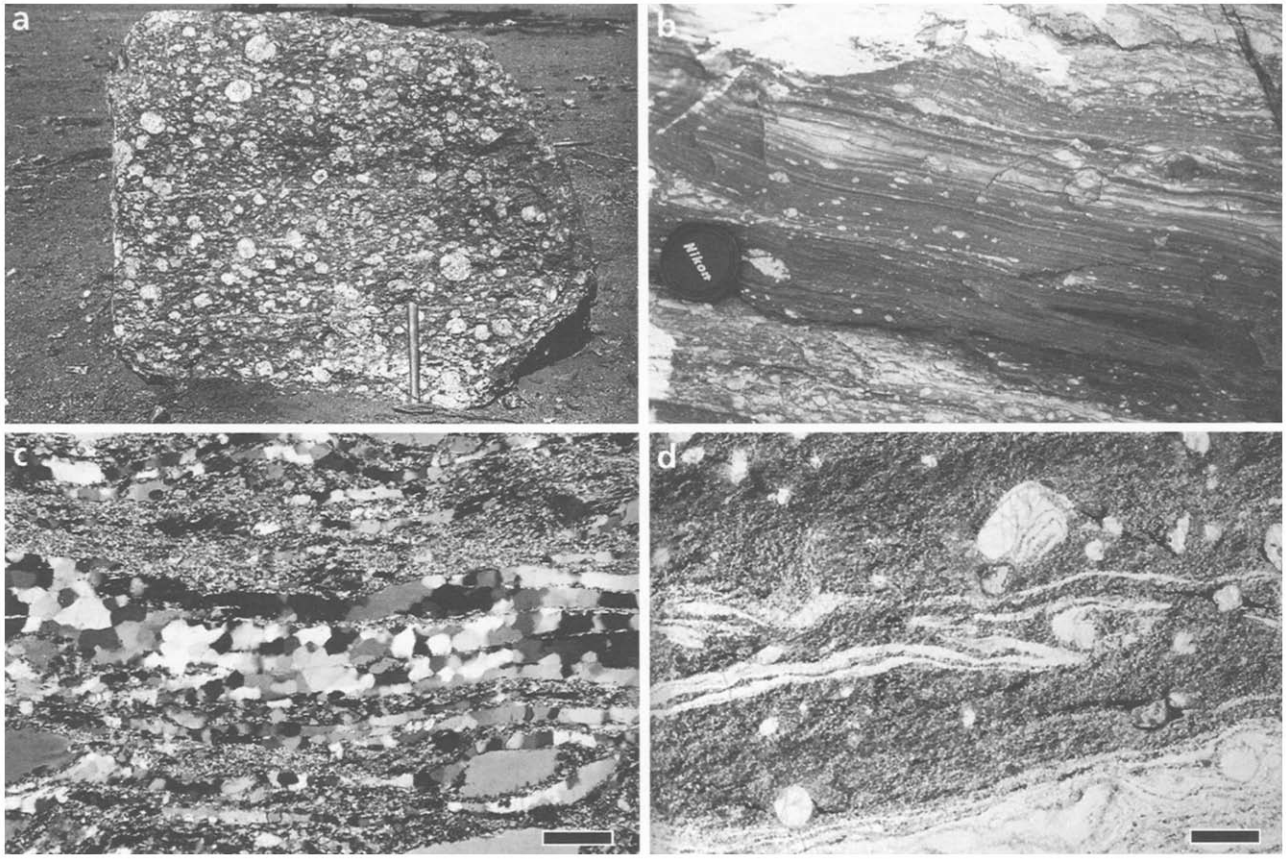

Fig. 2. (a) & (b) Field aspects of typical quartzo-feldspathic rocks of the Redbank Deformed Zone. (a) Coarse-grained country rock (weakly foliated granitic gneiss) in which the studied shear zones are developed. Feldspar clasts may be up to 30 cm in diameter. (b) Fine-grained amphibolite-facies quartzo-feldspathic ultramylonite south of Redbank Hill. Note that feldspar clasts characteristic of the protomylonites and mylonites tend to be absent in the ultramylonites. (c) & (d) Optical micrographs of pure quartz band microstructures in the amphibolite-facies shear zone studied. (c) Typical mylonite characterized by an alternation of pure quartz bands with quartz–feldspar bands. The pure quartz bands are made up of a coarse-grained (60 μm) recrystallized mosaic (crossed nicols, CN). Scale bar: 100 μm. (d) Small-scale folding of pure quartz bands (PPL) in an ultramylonite. Note the variations in thickness of the quartz bands. Scale bar: 300 μm.

the ultramylonites only a few small feldspar augen remain in a fine-grained matrix. These rocks have a black or very dark grey colour in hand specimen (Fig. 2b). This change in microstructure in both mylonite zones is accompanied by a decrease in the dip of the foliation: from 60–70°N in the protomylonites and weakly foliated country rock, via 50–55°N in the mylonites, to dips of 40–45°N in the ultramylonitic shear-zone centre (Figs 3a & 13a).

EXPERIMENTAL AND ANALYTICAL TECHNIQUES

All thin sections of the studied specimens were oriented to contain both the normal to the foliation and the stretching lineation. Grain size, grain shape and phase distribution analyses were carried out in SEM and optical microscopy. Mineral chemical analysis were performed in a microprobe, while TEM was used for the determina-

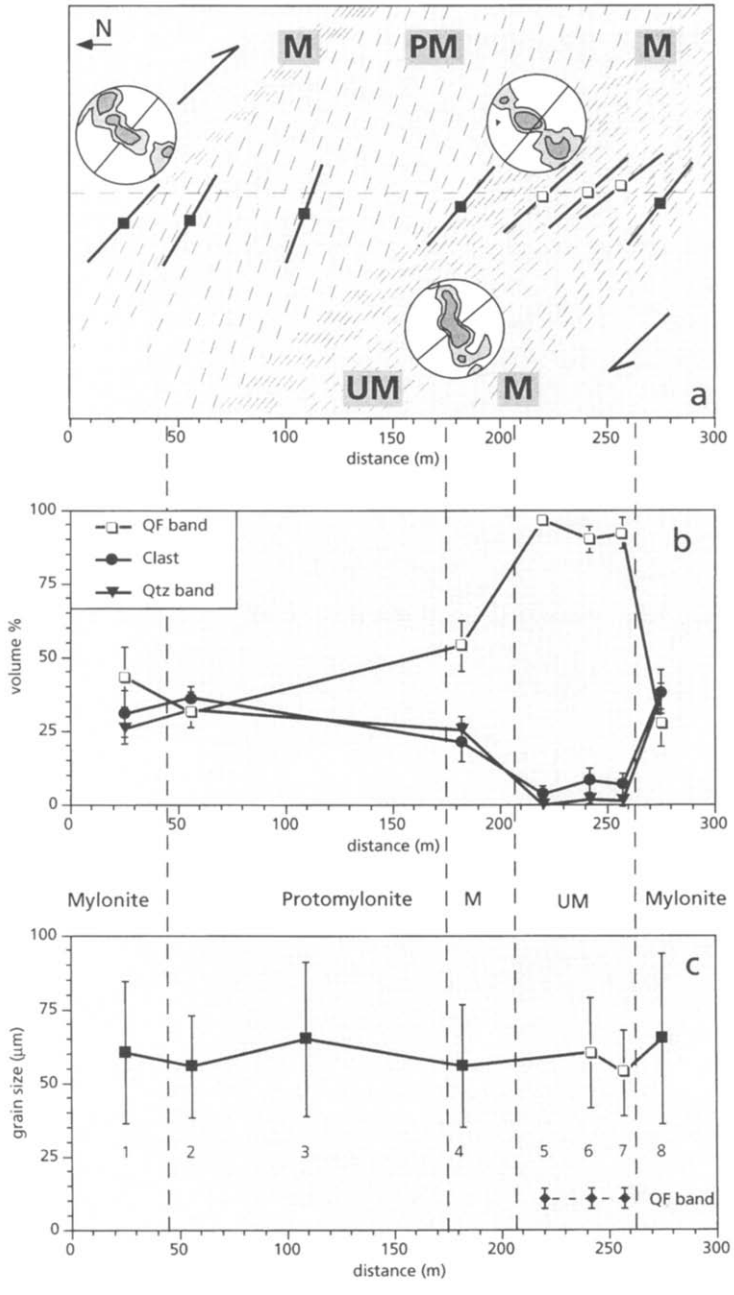

Fig. 3. Variations of microstructural features within the amphibolite-grade shear zone studied. (a) Schematic cross-section showing the orientation of the mylonitic foliation. Open symbols denote ultramylonitic rocks; closed symbols denote encapitulating protomylonitic and mylonitic rocks. Quartz *c*-axis textures of the pure quartz bands are shown; contours drawn at 2σ; $N=203$, $N=150$ and $N=100$. (b) Variation of the quartz–feldspar band (QF), pure quartz band (Q) and K-feldspar and plagioclase clast (C) content. (c) Variation of the median grain size of pure quartz bands, error bars represent half the interquartile range; the grain size of the QF bands are also indicated. PM, M, UM denote protomylonitic, mylonitic and ultramylonitic parts of the mylonite zone studied.

tion of the interfacial and intracrystalline microstructures. Details of the techniques used are presented in the Appendix. The extremely fine grain size of the greenschist-facies ultramylonite (average of 0.5 μm) hindered detailed SEM, and TEM has been used exclusively. Where grain sizes permitted, *c*-axis orientations of the pure quartz bands were measured using conventional U-stage techniques (Turner and Weiss, 1963). Otherwise, textures have been measured with both SEM electron back-scatter diffraction (EBSD) and TEM microdiffraction techniques.

In this paper an interface between two grains of a similar phase is referred to as a 'grain boundary', whereas a boundary between two dissimilar phases is called an 'interphase boundary'. The term grain-boundary sliding (GBS) denotes, unless specifically stated otherwise, sliding along both grain and interphase boundaries.

MICROSTRUCTURE OF THE AMPHIBOLITE-FACIES MYLONITE ZONE

Protomylonites and mylonites

The country rock in which the studied mylonite zone has developed is a foliated granitic gneiss with large feldspar augen and is referred to as protomylonite. A summary of the microstructural variations across the entire zone is provided in Table 1.

Both the protomylonitic and mylonitic rocks consist of porphyroclasts (20–40% of the rock volume) of K-feldspar ($Or_{92.6}$) and of plagioclase ($An_{38.3}$) embedded in a fine-grained foliated matrix (Fig. 4a). Ilmenite, monazite and rare allanite occur as accessory phases. The feldspar porphyroclasts commonly show weak undulatory extinction and subgrain formation, and usually have tails aligned parallel to the foliation. The clasts have a homogeneous mineral composition and show no exsolution. Within these rocks, most of the quartz occurs in discrete zones, 50–1000 μm thick, parallel to the foliation (Figs 2c & 4a). These pure quartz bands (60 μm grain size) alternate with continuous bands of finer-grained (5–11 μm) K-feldspar, plagioclase, quartz and biotite ± garnet, hereafter called quartz–feldspar bands (Fig. 2c). The matrix K-feldspar is more orthoclase-rich ($Or_{94.2}$) and the plagioclase is poorer in anorthite ($An_{33.5}$) compared to the porphyroclasts. All of the K-feldspar and plagioclase porphyroclasts are embedded within and mantled by these quartz–feldspar bands. The modal mineral composition of these bands is variable in that K-feldspar porphyroclasts may have tails composed of K-feldspar + biotite + quartz (KBQ in Fig. 4a) or of plagioclase + quartz + biotite (PQB in Fig. 4a). Similar observations are made on tails extending from plagioclase clasts. Some breakdown of feldspar clasts to a mixture of feldspar + biotite + quartz has been observed (Fig. 4a). Some euhedral garnet (< 50 μm) has been observed.

Polyphase ultramylonite

Towards the shear-zone centre the rock type progressively changes to a 40–50 m wide homogeneously mixed ultramylonite (Fig. 3). At the microscale, this change results from a progressive increase in vol. % of quartz–feldspar bands allied with a decrease in the vol. % of both the pure quartz bands and the K-feldspar and plagioclase porphyroclasts (compare Fig. 4a with Fig. 4b). Along with this increase is an increase in the thickness of the rim around the porphyroclasts. Sparse epidote may also occur within the ultramylonite. Although the modal mineral content of the thin (< 200 μm) quartz–feldspar bands of the protomylonitic and mylonitic rocks is quite variable (Fig. 4a), the ultramylonite matrix has a fairly constant modal mineral content of 40% quartz, 25% K-feldspar ($Or_{94.0}$), 25% plagioclase ($An_{37.7}$) and 10%

Table 1. Summary of microstructures within the amphibolite-facies mylonite zone

Sample	1	2	3	4	5	6	7	8
% KF	15±6	15±3		10±5	1±1	3±3	3±5	26±10
% PL	16±8	21±4		12±7	3±3	5±4	4±3	11±8
% C	31±8	36±4		21±6	4±3	8±4	7±4	37±8
% QF	43±10	32±5		54±8	96±3	90±4	92±5	26±6
% Q	26±5	32±6	100	25±5	0	2±1	1±2	36±5
% rim	14±7	10±6		25±9	96±3	92±3	92±5	9±6
D_{qtz}	60±24	56±17	65±26	56±21		60±19	53±15	65±29
Sk	1.6	1.7	2.0	1.5		2.1	1.7	1.4
Km	3.7	4.1	6.1	2.8		6.2	4.1	3.9
D_{QF}					11±4	11±4	11±4	
Sk					0.4	0.4	0.4	
Km					−0.5	−0.5	−0.5	
K	0.2			0.2	(0.5)	0.4		
C	2.2			2.0	(1.0)	2.8		

Key: % KF, vol. % K-feldspar clast; % PL, vol. % plagioclase clast; % C, total vol. % porphyroclasts; % QF, vol. % quartz–feldspar band; % Q, vol. % pure quartz bands; % rim, vol. % rim around porphyroclast. D_{qtz}, grain size of pure quartz ribbons; D_{QF}, grain size of quartz–feldspar bands; *Sk* and *Km*, skewness and kurtosis, respectively; *K* and *C*, shape and strength of pure quartz band *c*-axis texture, respectively. The values for quartz within the polyphase ultramylonites are given between parentheses. Sample numbers refer to those in Fig. 3(a).

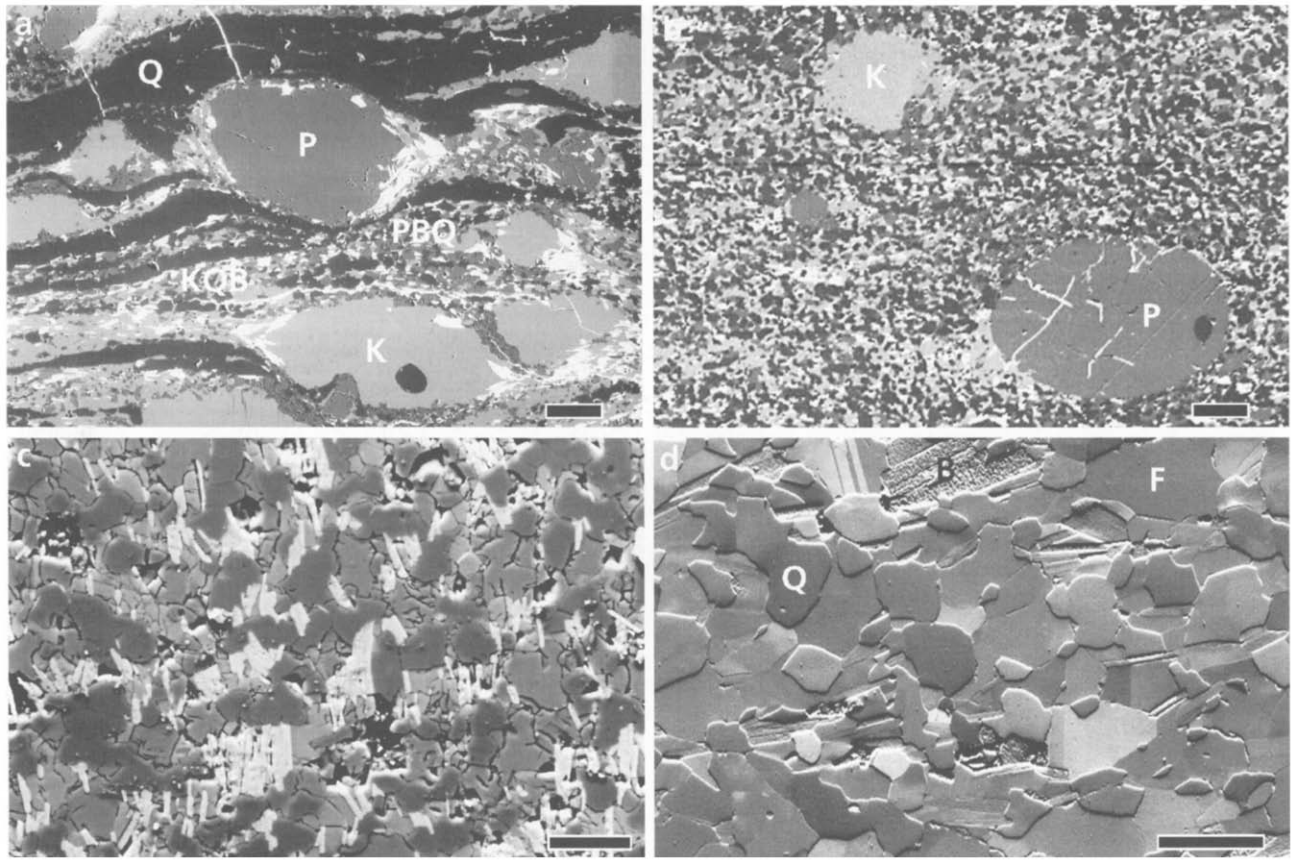

Fig. 4. SEM images of typical microstructures in the amphibolite-facies shear zone. (a) BSE image of a mylonite showing porphyroclasts of plagioclase (P) and K-feldspar (K) embedded in a matrix of finer-grained bands of K-feldspar, plagioclase, quartz and biotite, alternating with pure quartz bands (Q). K-feldspar might be surrounded by very fine-grained (5–11 μm) K-feldspar, quartz and biotite (marked as KQB) or by plagioclase, quartz and biotite (marked as PBQ). Scale bar: 100 μm. (b) BSE micrograph of an ultramylonite showing porphyroclasts of K-feldspar (K) and plagioclase (P) embedded in a fine-grained (5–11 μm) homogeneous polyphase matrix. Note the decrease in size and number of both the K-feldspar and plagioclase clasts, and the increase in quartz–feldspar band content in the ultramylonite. Scale bar: 100 μm. (c) Higher magnification BSE micrograph of a polished and etched ultramylonite. Minerals in order of brightness are biotite (brightest), K-feldspar, plagioclase and quartz (darkest). Holes in the sample appear black. Foliation is parallel to the short side of the micrograph. Scale bar: 30 μm. (d) OCI showing the microstructure of the ultramylonite. Owing to polishing the quartz grains have a high relief, both the K-feldspar and plagioclase have a low relief, biotite is lath-shaped. Scale bar: 5 μm. The white dots are remnants of the polishing medium.

biotite (Fig. 4b). Garnet occurs as skeletal clusters of individual grains and appear syn-deformation. A summary of the microstructural elements is provided in Table 2.

Table 2. Summary of the microstructural characteristics of the amphibolite-facies ultramylonite (sample 5)

	K-feldspar	Plagioclase	Quartz	Biotite
Vol. %	25	25	40	10
D	6.5±2.5	6.8±3.7	10.8±3.6	5.4±2.4
Sk	0.7	1.0	0.4	0.6
Km	1.1	0.5	−0.5	0.7
C	0.8±0.1	0.8±0.1	0.8±0.1	0.7±0.2
E	1.9±0.4	1.8±0.4	1.5±0.3	2.9±1.2
SF	0.9±0.1	0.9±0.1	0.9±0.0	0.8±0.1
N	170	134	158	245

Key: *D*, grain size in μm; *Sk* and *Km*, skewness and kurtosis, respectively; *C*, circularity; *E*, elongation; *SF*, shape factor; *N*, number of measurements.

The grain sizes of the minerals are uniformly small. That of the biotite is 5 ± 2 μm, K-feldspar is 7 ± 3 μm, plagioclase is 7 ± 4 μm and quartz is 11 ± 4 μm. The grains have a rectangular to square grain shape (Figs 4c & 5), and are elongated (sub)parallel to the long axes of the mica laths, which define the foliation (Fig. 5b). There is no major difference between the grain shapes of the plagioclase, K-feldspar and the quartz grains as expressed by their circularity, elongation and shape factor (Table 2). The elongation of quartz grains ($E=1.5\pm0.3$) is somewhat less compared to the elongation of the plagioclase ($E=1.8\pm0.4$) and K-feldspar ($E=1.9\pm0.4$). Small domains consisting only of plagioclase or K-feldspar or of a two-feldspar mixture are occasionally observed within the ultramylonite. These domains have grain sizes (5–11 μm) similar to those of the quartz–feldspar bands in the mylonitic rocks and to those of the four-phase matrix, suggesting that the feldspar grain sizes are stable. The quartz grain size, however, is

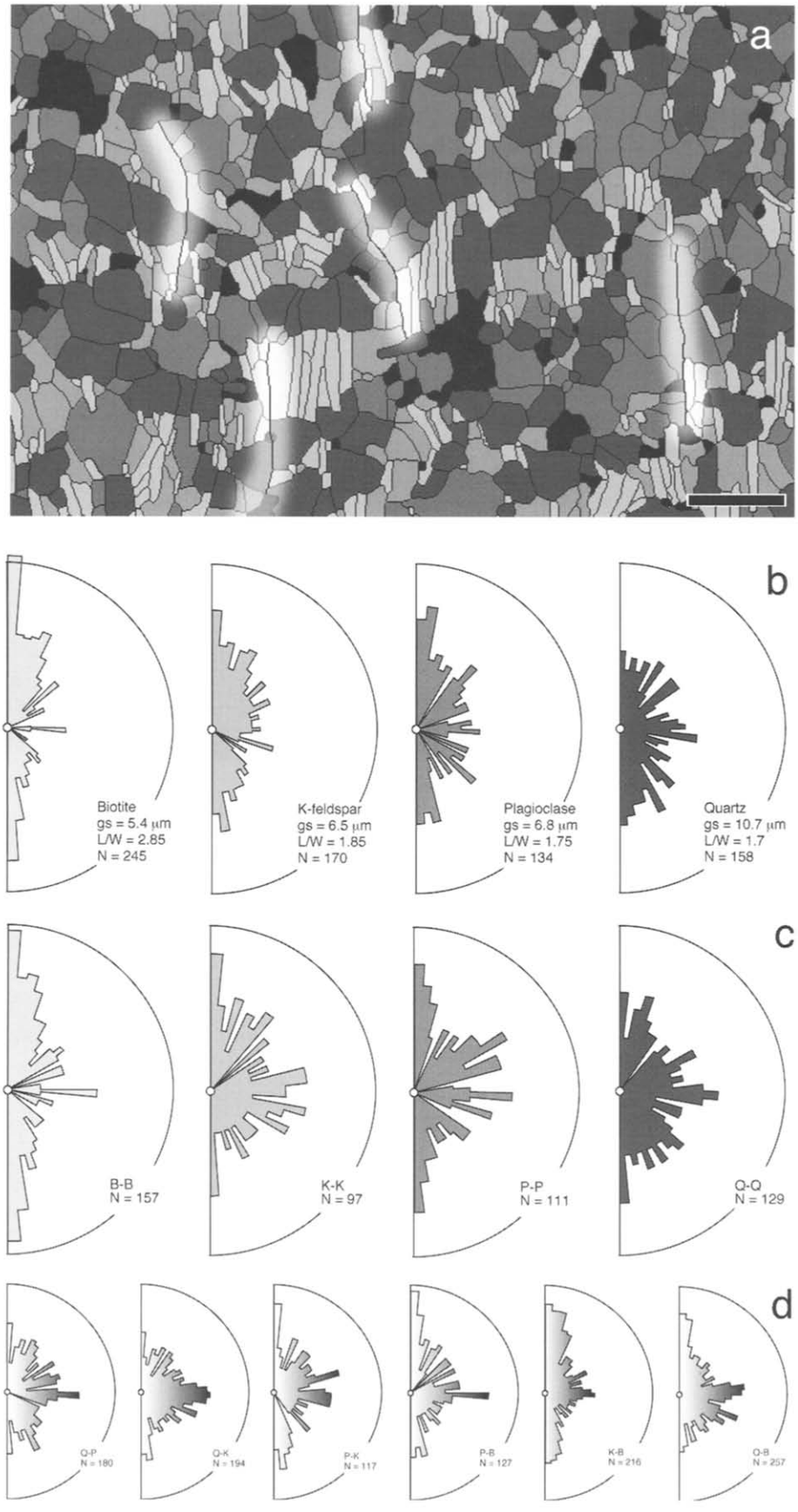

Fig. 5. (a) Line drawing after Fig. 4(c) showing the continuous alignment of grain and interphase boundaries across several grain diameters; several of them are highlighted. Scale bar: 30 μm. Minerals are shaded in brightness similar to that of Fig. 4(c). (b) Rose diagram showing the orientation of the long axis of the grain with respect to the short side of the photograph. (c) & (d) Rose diagrams showing the orientation of the traces of the (c) grain boundaries and (d) interphase boundaries. gs, grain size; *N*, number of observations. Grey scales correspond to those in (a). B, biotite; K, K-feldspar; P, plagioclase; Q, quartz.

much smaller than that of the pure quartz bands (60 ± 19 μm, see the next section).

The orientation distributions of the grain and interphase boundaries are shown as rose diagrams in Fig. 5(c & d). Both the grain and interphase boundaries show a preferred alignment parallel to the foliation, with a second alignment perpendicular to this direction, resulting in a blocky grain shape. Long grain boundaries occur mainly parallel to the foliation (Fig. 5a). Many grain and interphase boundaries are interlinked parallel to the foliation and are continuously aligned across several grain diameters (Fig. 5). However, not all grain and interphase boundaries link up, and the continuous boundaries have a limited extent (up to 100 μm). The average length of these continuous boundaries is 37 ± 18 μm. Therefore, with an average grain size between 5 and 11 μm, four–six adjoining grains make up such a continuous boundary. The average spacing between these continuous grain boundaries is 16 ± 4 μm, which equals two–three grain diameters.

Microstructures and textures (CPO) in the pure quartz bands

Bands of pure quartz occur mainly in the protomylonites and mylonites, they are very rare in the ultramylonites (Fig. 3). These pure quartz bands although long (up to several cm) are not continuous and appear to laterally thin (Fig. 2d). Small-scale folding of the bands occurs primarily within the ultramylonitic shear-zone centre (Fig. 2d), whereas folding was not seen within the mylonitic rocks. Many of the folds are asymmetric with cuspate fold hinges (Fig. 2d). The ratio of folded to unfolded quartz bands is approximately 0.5. Concomitantly, pure quartz bands within the ultramylonites show variations in the thickness of the bands (Fig. 2d), whereas in the (proto)mylonitic rocks pure quartz and quartz–feldspar bands anastomose around the feldspar augen.

Quartz occurs as slightly elongated polygonal grains. They show abundant undulatory extinction, subgrain formation (20 ± 5 μm) and serrated grain boundaries (Fig. 2c). The grain sizes of the quartz remains constant across the mylonite zone at around 60 μm (ranging from 53 to 65 μm) (Fig. 3c and Table 1). Note, however, that in the pure quartz bands in the ultramylonitic centre of the shear zones, the average grain size is about half the width of the quartz bands in question, which will limit the size of the constituent grains.

Figure 3(a) shows the variation of *c*-axis textures of the pure quartz bands across the mylonite zone. All *c*-axis textures are type 1 girdles (Lister, 1977) (texture shape factor (K) = 0.2–0.4; strength of the distribution (C) = 2.0–2.8). Those measured in the protomylonitic and mylonitic rocks are symmetrically arranged to the foliation, whereas the texture in the ultramylonite shows a marked asymmetry consistent with a reverse movement along the shear zone. The pole figures are similar to quartz *c*-axis textures previously measured in similar rock types of similar metamorphic grade along the Redbank Deformed Zone (Obee and White, 1986). The microstructures and strong textures suggest that deformation in these pure quartz bands involved a major contribution of dislocation-creep mechanisms.

Temperature estimates

The mineral assemblage within the matrix of the samples is typical for that expected from rocks of granodioritic bulk composition metamorphosed under almandine–amphibiolite-facies conditions (Turner, 1968, fig. 7-27). This is confirmed by application of the garnet–biotite Fe–Mg exchange thermometer of Kleemann and Reinhardt (1994), which yields temperatures of around 600 ± 75°C. The occurrence of epidote and skeletal garnet in the ultramylonitic matrix as opposed to the absence of epidote in the (proto)mylonites indicates slightly lower temperatures for the former compared to the latter (Turner, 1968, fig. 7-25). As the homogeneous phases comprise the deformed rock matrix, it is assumed that deformation occurred at these conditions, i.e. under amphibolite-facies conditions. These temperature estimates are comparable to those reported by Shaw and Black (1991) in similar shear zones within the Redbank Deformed Zone.

QUARTZ MICROTEXTURE OF THE AMPHIBOLITE-FACIES POLYPHASE ULTRAMYLONITE

Crystallographic preferred orientation (CPO)

A representative area of the amphibolite-facies polyphase ultramylonite showing an orientation contrast is shown in Fig. 4(d). Because of differential polishing rates of the minerals during the colloidal silica polishing some relief is present; quartz appears to be the most resistant mineral. Consequently, quartz grains are easy to identify and all grains in an area can be analysed. The results of the texture analyses of quartz from the polyphase amphibolite-facies ultramylonite, using the EBSD technique in SEM, are shown in Fig. 6. Only the *c*-axes show a very weak preferred orientation into a broad maximum in the centre of the pole figure (Fig. 6a). The *a*-axes (Fig. 6b) and the normals to both the positive (r) and negative (z) rhombohedral planes (Fig. 6c & d) are randomly distributed. The eigenvalue method tests for randomness show that for all axes the strength of the distribution, C, is very low (*c*-axes, 0.5; *a*-axes, 0.2; both the rhombohedral planes, 0). The texture shape factor, K, is close to 1 for all axes. The *c*-axis texture is quite different to the ones obtained optically from the pure (60 μm) quartz bands (Fig. 3), which are strong girdle distributions slightly asymmetric to the foliation.

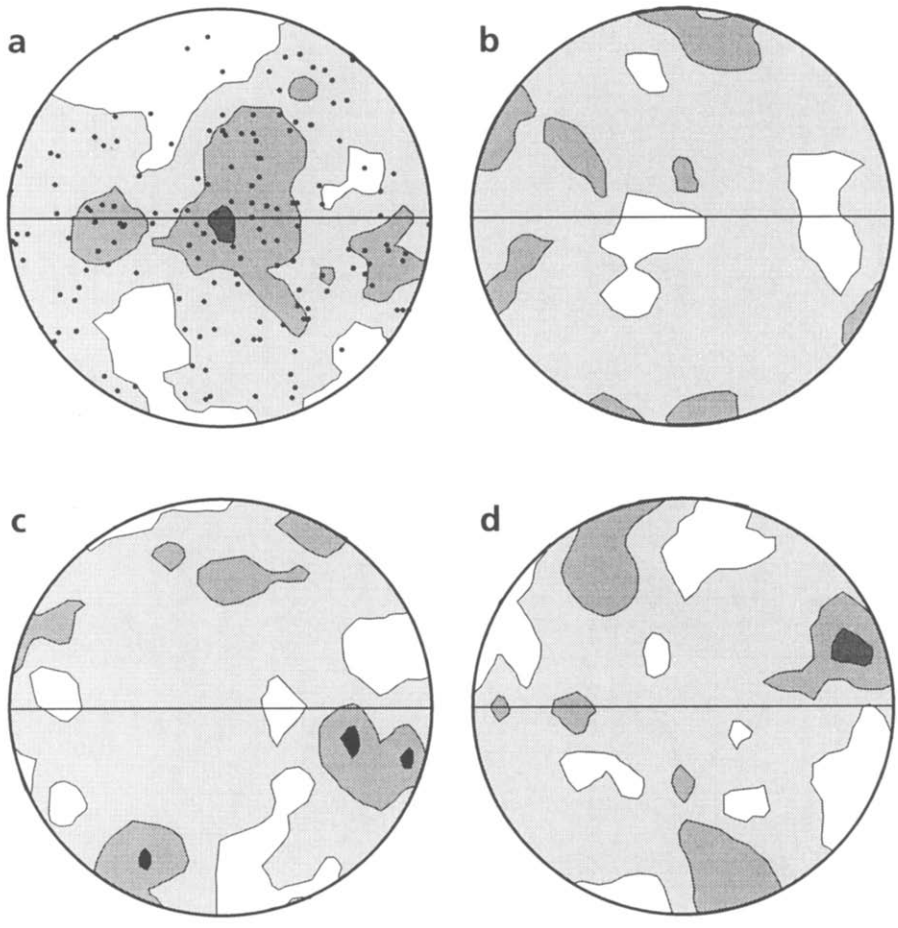

Fig. 6. Pole figures showing the weak texture of quartz grains from the amphibolite-grade ultramylonite as measured with the EBSD technique in SEM: (a) *c*-axes; (b) *a*-axes; normals to (c) *r* (+) and (d) *z*(−) rhombohedral planes. $N = 160$. Contours drawn at 2σ. The foliation is horizontal and the stretching lineation is on the foliation plane at the edge of the pole figure.

Misorientation relationships

Uncorrelated or random misorientations. By taking the misorientation with the smallest possible angle, certain combinations of axes–angle may occur more frequently than others. For quartz, with its trigonal symmetry, at high rotation angles ($> 60°$) certain misorientation axes are forbidden; these are displayed in Fig. 7(d) as shaded areas (Heidelbach, 1994). Similar forbidden areas occur in cubic materials (Heinz and Neumann, 1991; Heidelbach, 1994) and in orthorhombic materials (Grimmer, 1989). Therefore, in the inverse pole figure displaying the axes–angle pairs with very high angles ($> 60°$), there is a natural tendency for a high density area near the bottom of the pole figure close to [$6\bar{2}41$] (Fig. 7d).

Furthermore, the distribution of angles of misorientation between adjacent grains will not be uniform (Heinz and Neumann, 1991; Randle, 1993; Heidelbach, 1994). As pointed out by Randle (1993), only if the crystals are triclinic will a random distribution of misorientations give rise to a uniform distribution, i.e. in which each misorientation angle can occur equally frequently. This is because in the triclinic case each individual misorientation can be described by only one axis–angle pair. This anisotropic density distribution of misorientations makes it difficult to assess visually when a misorientation distribution (MOD) is random. Even more, when describing and comparing MODs, it should be first known which misorientation relations are possible and which are not. Although it is possible to calculate the forbidden misorientations, the calculation is not straightforward (Heinz and Neumann, 1991). Therefore, a simpler approach has been adopted in this study and is given below.

It is assumed that the quartz texture within the polyphase ultramylonite as presented in Fig. 6 is random. From this texture dataset, 3000 grain–grain pairs were selected at random and the misorientation was calculated. This new dataset includes grains that are physically adjacent to each other and grains which are apart. It is assumed that such a MOD represents the distribution of axes–angles pairs for the case of statistically random misorientation. Mainprice *et al.* (1993) refers to such a distribution as the uncorrelated MOD. The resultant distribution of angles of misorientation is shown as a thin line in Fig. 7(a). It can be clearly seen that there is a tendency towards higher frequencies for the larger angles, with a maximum around 60–80°. A similar distribution has been reported for cubic materials

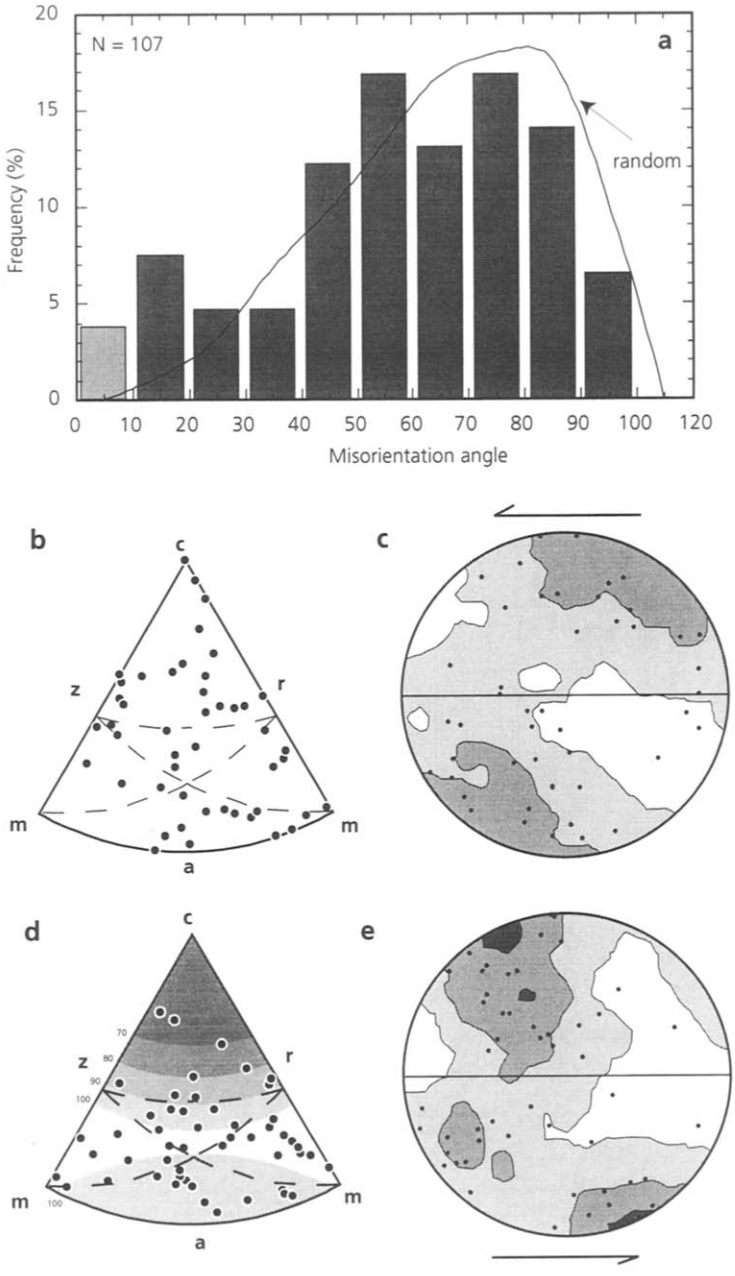

Fig. 7. Misorientation distribution analysis between quartz grains encountered in the amphibolite-grade ultramylonite. (a) Distribution of angles of misorientation between adjacent quartz grains, subgrains are shown in brighter tones; $N = 107$. Also shown, as a thin line marked random, is the distribution of the uncorrelated misorientation distribution (see text for discussion). (b) & (d) Inverse pole figures and (c) & (e) pole figures of the axes of finite misorientation between adjacent quartz grains, the sense of shear is left-lateral. (b) & (c) Axes of misorientation between grains with a low to intermediate (10–60°) angle of misorientation. They are randomly distributed in crystal coordinates (b), but define a broad maximum lying at the edge of the pole figure inclined 60° to the foliation away from the direction of shear. (d) The axes between grains with a high angle ($> 60°$) of misorientation are randomly distributed in crystal coordinates. Forbidden orientations for misorientation axes with a certain misorientation angle are indicated with a grey scale (see text for discussion). (e) Demonstrating a preferred orientation at 60°to the foliation, towards the direction of shear.

(Haessner *et al.*, 1983), where a maximum occurs around 45°. Therefore, as this uncorrelated or random MOD contains all possible misorientations, the observed MOD should be compared to this.

Correlated or observed misorientations. The distribution of angles of misorientation between adjacent quartz grains is presented as a bar-graph in Fig. 7(a). Boundaries with less then 10° of misorientation across are treated as being subgrain boundaries (White, 1976). It can be seen that the distribution is not uniform across all angles. There are more grain boundaries having high to very high misorientations compared to grain boundaries with low to intermediate misorientation

angles. The observed angular distribution follows the trend depicted by the uncorrelated MOD. Comparing the observed and uncorrelated distribution, whereby omitting misorientations $<10°$ (i.e. the subgrains) results in a χ^2 test of 41.3. This test value exceeds the critical value of χ^2 at 5% significance, which is 12.6, so it can be concluded that the uncorrelated and observed distributions are different. All of this difference is accounted for by the boundaries having an angle of misorientation between 10° and 20°. Except for the low angle boundaries ($<20°$), the observed distribution is not significantly different to the statistically random case.

The MOD has been divided into two sets of roughly equal data density. One (46% of the data) contains intermediate angle boundaries ranging from 10° to 60°, whereas the other (51% of the data) contains the high angle boundary data ($>60°$). The commonly used division in 5° intervals (cf. Randle, 1992, 1993; Heidelbach, 1994) is not used here, as the classes for the low and medium angles contain too few data to be statistically relevant.

Representing the axes of misorientation between adjacent quartz grains in crystal coordinates, neither the low to intermediate nor the high angle boundaries show a strong preferred orientation in great-circle girdles or point maxima (Fig. 7b & d). However, in specimen coordinates, weak preferred orientations of misorientation axes do occur. The axes of misorientation between adjacent grains having low to intermediate angles (Fig. 7c) define a broad maximum ($C=0.6$; $K=1.9$) lying at the edge of the pole figure inclined at 60° to the foliation with an asymmetry opposite to the sense of shear. The axes between grains, having high angles of misorientation (Fig. 7e), also show a (stronger) preferred orientation ($C=0.8$; $K=1.9$) at 60° to the foliation, but now with an asymmetry similar to the sense of shear. The reason for this preferred alignment of the misorientation axes in specimen coordinates is at present unclear. As it only occurs in specimen coordinates and not in crystal coordinates, it is suggested to be related to the macroscopic shear and not to a crystallographic property.

Coincidence site lattices. The misorientation relations between grains were tested against the coincidence site lattice (CSL) theory for trigonal crystals (see for details McLaren, 1986, table 3; Grimmer, 1989; Mainprice *et al.*, 1993; Fliervoet and White, 1995). In a CSL orientation, the fraction of lattice points of the two crystals that coincide is given as $1/\Sigma$ (Grimmer, 1989; Mainprice *et al.*, 1993). The smaller the value of Σ, the larger the coincidence and the better the 'fit' between the grains. In general, misorientations with a $\Sigma<49$ are considered to have a CSL (cf. Randle, 1993). Those with larger Σs are referred to as general boundaries. Brandon's criterion (cf. Randle, 1993) has been used to calculate the maximum deviation from a CSL misorientation.

For example, for quartz the Dauphiné twin law, i.e. a 60° rotation around the *c*-axis, is known to produce a CSL misorientation with $\Sigma=3$ (McLaren, 1986; Grimmer, 1989; Mainprice *et al.*, 1993); other CSL relations calculated for quartz are mainly based on the other twin laws and are given by McLaren (1986), table 3. Only misorientations with axes parallel to an *a*-axis, the *c*-axis or normal to an *m* plane can produce CSL misorientations (McLaren, 1986; Grimmer, 1989). When the misorientation data presented in Fig. 7 are compared with the CSL relations for quartz it is found that only 10% of the misorientation relations can be described as having a CSL with a Σ value lower than 49. The remaining 90% are random, or general, grain boundaries.

TRANSMISSION ELECTRON MICROSCOPY OF AMPHIBOLITE-GRADE POLYPHASE ULTRAMYLONITE

Intracrystalline defect structures

The lattice-scale deformation microstructures of quartz, K-feldspar and plagioclase from the fine-grained polyphase ultramylonite have been studied using TEM. At this scale (Fig. 8) the free dislocations within quartz are commonly straight or curved and are decorated with small inclusions (median $=0.05\pm0.01$ μm; skewness (Sk) $=-0.26$; kurtosis (Km) $=-0.53$). These inclusions have an ovoid to negative crystal shape and show a contrast consistent with that expected from fluid bubbles or voids (Edington, 1974; McLaren, 1991). Trace analyses were carried out on these curved dislocations and reveal that these dislocations lie mainly on rhombohedral and basal planes and, less commonly, on prism planes (Fig. 9). Dislocations tend to be curved in areas of high bubble density (Fig. 8a). The free dislocation density (median $=5.9\pm2.7\times10^{12}$ cm^{-2}; $Sk=0.02$; $Km=-1.06$) varies inhomogeneously through the sample. There is a general association of high dislocation densities with high bubble density. Defect-free quartz grains have been observed; no set relation between quartz grain orientation and defect density has been observed.

Within the larger grains (typically >15 μm) some subgrain boundaries (Fig. 8b) and dislocation arrays (Fig. 8c) have been observed which are preferentially aligned either parallel or perpendicular to the foliation. These boundaries generally have an orientation close to a rhombohedral or prism plane orientation (Fig. 8c).

Most of the plagioclase and K-feldspar grains have no dislocations and/or bubbles; some planar defects occur within K-feldspar (Fig. 10a). These planar defects might be interpreted either as twin boundaries or healed microcracks, as the diffraction contrast changes on opposite sides of the boundary (Edington, 1974; McLaren, 1991); however, no twin rotations have been observed in the diffraction patterns.

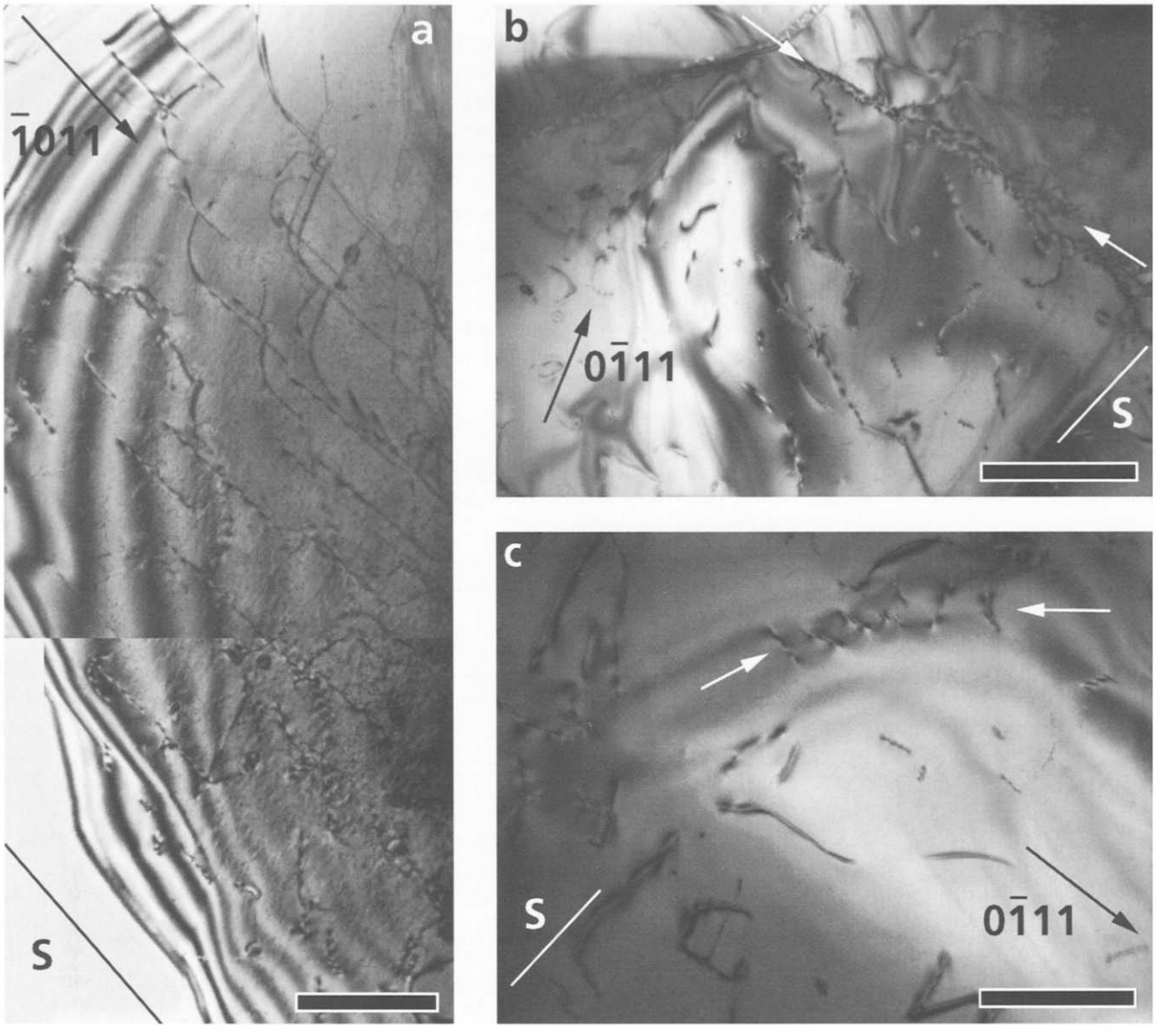

Fig. 8. TEM BF micrographs showing intracrystalline defect structures of quartz. (a) Substructure in an area of high dislocation density. The dislocations are decorated with bubbles. (b) Area having a medium dislocation density with a subgrain wall (arrowed). (c) Area of low dislocation density with dislocation array. The orientation of the foliation is marked (S). All scale bars are 1 μm.

Intercrystalline defect structures

Many of the quartz–quartz grain boundaries contain voids. Some parallel to the foliation are decorated with arrays of asymmetric, sigmoidal-shaped voids (Fig. 10b). Analysis of quartz–quartz grain-boundary plane normals show no PO (Fig. 11c); both the boundaries perpendicular and parallel to the foliation are scattered in the inverse pole figure.

Although the majority of interphase boundaries are straight and either parallel or perpendicular to the foliation (Fig. 10a), curved interphase boundaries have been observed, an example is given in Fig. 10(c). Here the interphase boundary between a K-feldspar and a quartz grain curves towards both the quartz and the K-feldspar.

Quartz microtexture analyses

We have measured texture and MOD by TEM of fine-grained (2.3 μm) quartz bands in similar rock types (data and analyses are presented in Fliervoet and White, 1995). The quartz *c*-axis texture is strong and similar to that of the pure quartz bands in the amphibolite-grade mylonites. For comparison, we have also measured the quartz texture in the ultramylonites with TEM. The CPO as measured with TEM is similar to that measured with the EBSD technique in SEM (compare Fig. 6 with Fig. 11a & b), this despite fewer measurements in TEM. The *c*-axes show a very weak maximum ($C=0.5$; $K=6.2$) near the centre of the pole figure (Fig. 11a), whereas the *a*-axes are randomly distributed ($C=0.3$; $K=0.1$) (Fig. 11b).

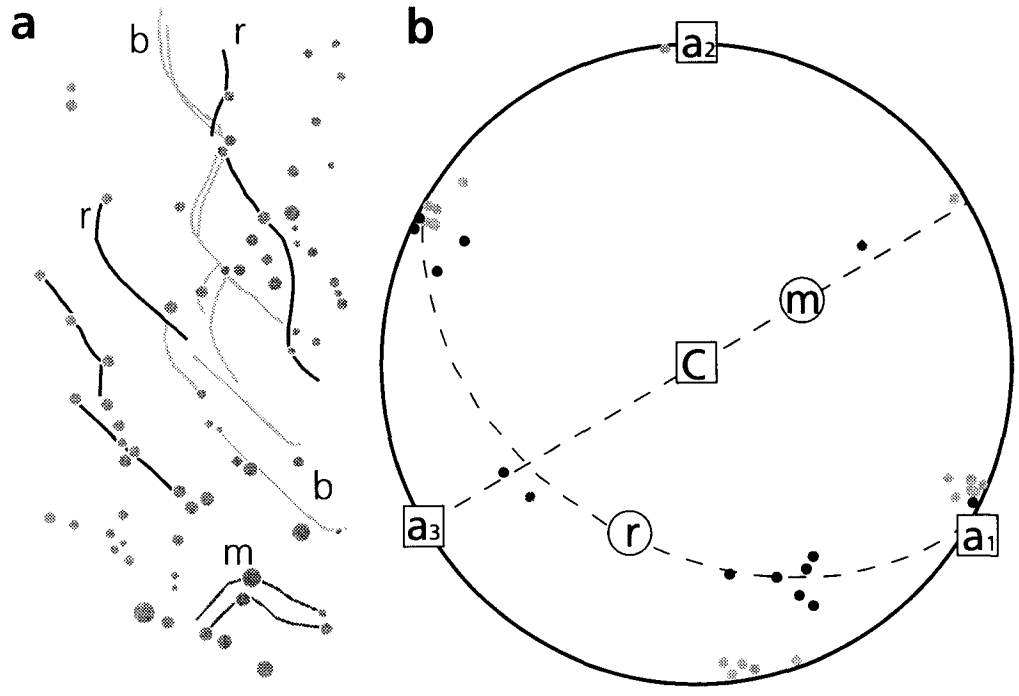

Fig. 9. Trace analysis on the bubble dislocation system of Fig. 8(a). (a) Sketch showing the dislocations (lines) and bubbles (circles). (b) Stereogram showing the orientation of the dislocation lines. Key: light grey, dislocations lying on a basal plane; medium grey, dislocations lying on a *m* prism (*m*) plane; dark grey, dislocations lying on a rhombohedral (*r*) plane.

Figure 12(a) shows the distribution of angles of misorientation between adjacent quartz grains. The statistically random case could not be calculated due to too few data. However, in a random misorientation distribution between hexagonal crystals, a maximum is expected between 30 and 70°; the maximum angle is 93.8° around an axes close to [$6\bar{2}41$], i.e. away from the *c*-axis (Grimmer, 1980). Omitting the subgrains encountered, the distribution of angles between quartz grains in the polyphase ultramylonites shows a fairly uniform distribution with a maximum between 40 and 60°, and a tendency for higher angle boundaries. However, the distribution of angles of misorientation between adjacent quartz grains in the fine-grained (2.3 μm) pure quartz bands within the greenschist-grade ultramylonite (Fig. 12b), is very different in that low and intermediate angles are favoured (see discussion below).

The distribution of axes of misorientation between adjacent grains in crystal coordinates shows a tendency to plot away from the *c*-axis (Fig. 11d). Because of too few measurements, no distinction between low to intermediate and high angle boundaries could be made. As noted previously, this is thought to reflect the 'natural tendency' of a random distribution having a pole-free area near the *c*-axis. No obvious preferred orientation can be seen when the axes are plotted in specimen coordinates (Fig. 11e). Furthermore, as can be seen in Fig. 11(d & e), the axes of misorientation between grains with a boundary parallel to the foliation are as widely dispersed as axes between grains with their boundaries perpendicular to the foliation.

GREENSCHIST-FACIES MYLONITE ZONE

Microstructures within protomylonites and mylonites

The rock enclosing the greenschist-facies shear zone studied is similar to that of the amphibolite-facies mylonite zone: a foliated granitic gneiss with large feldspar augen. A summary of the microstructures across the zone is presented in Fig. 13 and Table 3.

Table 3. Summary of microstructures within the greenschist-facies mylonite zone

Sample	1	2	3
% KF	19±7	13±3	5±4
% PL	16±5	15±3	11±5
% C	35±4	28±8	15±8
% QF	34±9	49±11	72±11
% Q	31±5	23±5	13±4
% rim	13±10	21±11	83±5
D_{qtz}	31±9	2.3±0.8	
Sk	1.2	1.7	
Km	1.8	2.6	
D_{QF}			0.5±0.2
Sk			2.5
Km			7.8
K	0.1	0.6	
C	1.9	2.3	

Key: % KF, vol. % K-feldspar clast; % PL, vol. % plagioclase clast; % C, total vol. % porphyroclasts; % QF, vol. % quartz–feldspar band; % Q, vol. % pure quartz bands; % rim, vol. % rim around porphyroclast. D_{qtz}, grain size of pure quartz ribbons; D_{QF}, grain size of quartz–feldspar bands; *Sk* and *Km*, skewness and kurtosis, respectively; *K* and *C*, shape and strength of pure quartz band *c*-axis texture, respectively. Sample numbers refer to those in Fig. 13(a).

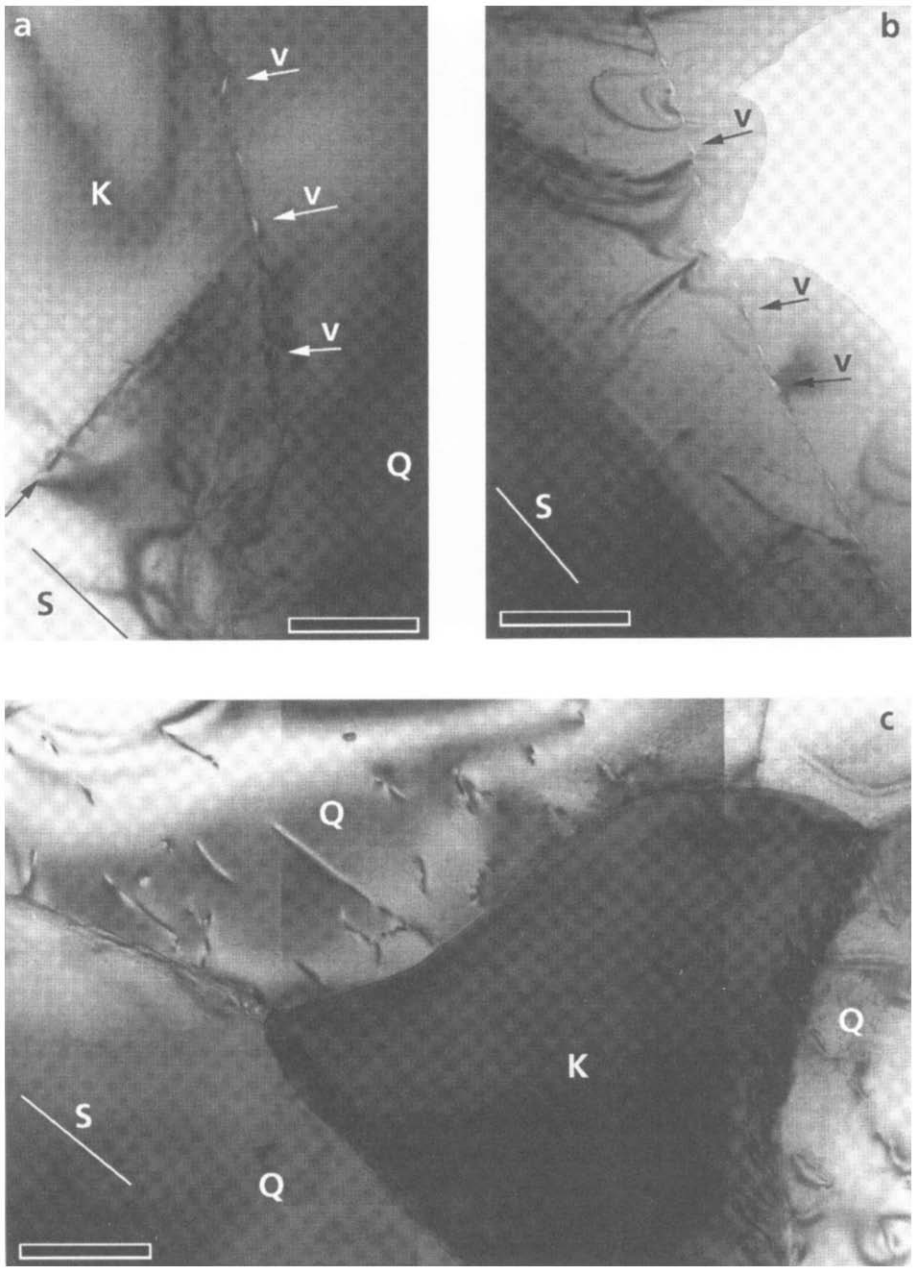

Fig. 10. TEM BF micrographs showing details of grain and interphase boundaries encountered in the amphibolite-facies ultramylonite. (a) Interphase boundary between a K-feldspar grain (K) and a quartz (Q) grain tilted parallel to the electron beam. The interphase boundary contains voids (small arrows marked v). (b) Quartz–quartz grain boundary decorated with asymmetric, sigmodial-shaped voids (labelled v). (c) Curved interphase boundary between quartz (Q) containing dislocations and a K-feldspar (K) grain. Scale bars: 1 μm. The orientation of the foliation is marked (S).

Similar to the amphibolite-facies mylonite zone, the protomylonitic and mylonitic rocks of the greenschist-facies shear zone consist of porphyroclasts (20–30% of the rock volume) of K-feldspar ($Or_{92.5}$), plagioclase ($An_{27.5}$) and epidote, embedded in a fine-grained foliated matrix (Fig. 14a). Garnet is absent, whereas sparse muscovite occurs. The porphyroclasts commonly show weak undulatory extinction, limited fracturing and limited subgrain formation, and commonly have tails aligned parallel to the foliation. The clasts have a homogeneous mineral composition, and the K-feldspar clasts show limited exsolution of sodic-plagioclase. Within these rocks, most of the quartz occurs in discrete zones, 10–200 μm thick, defining the foliation (Fig. 14a). These pure quartz bands (grain size 31 ± 9 μm; $Sk = 1.2$; $Km = 1.8$) alternate with continuous bands of finer-grained (0.5 ± 0.2 μm; $Sk = 2.5$; $Km = 7.8$) K-feldspar ($Or_{92.6}$), plagioclase ($An_{21.2}$), quartz and biotite, hereafter called quartz–feldspar bands (Fig. 14a). All of the K-feldspar and plagioclase porphyroclasts are embedded within and rimmed by these quartz–feldspar bands (Fig. 14a).

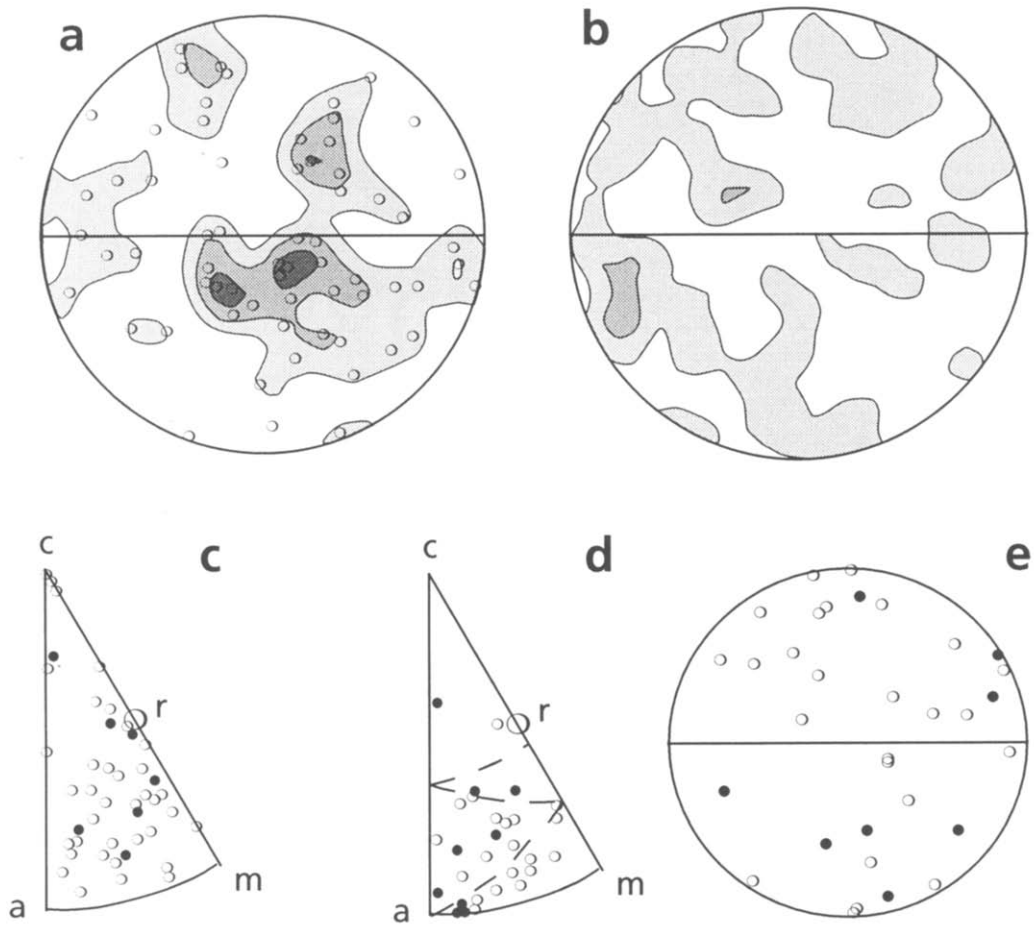

Fig. 11. TEM-based CPO and misorientation analysis of quartz grains from the amphibolite-grade ultramylonite. (a) & (b) Pole figures showing the weak texture of (a) *c*-axes and (b) *a*-axes. $N=65$. Contours drawn at 2σ. (c) Inverse pole figure showing the orientation of the normal to quartz–quartz grain boundaries with respect to both crystal lattices. (d) & (e) Axes of misorientation measured between grains presented in (d) an inverse pole figure and (e) a pole figure; in (e) the foliation is shown horizontal. Open and closed symbols denote boundaries parallel or perpendicular to the foliation, respectively. The foliation is horizontal and the stretching lineation is on the foliation plane at the edge of the pole figure. See text for discussion.

Microstructures within the polyphase ultramylonite

Towards the shear-zone centre the rock type progressively changes to a 5–10 cm wide ultramylonite (Fig. 13). At the microscale, this change is accompanied by a progressive increase in vol. % of quartz–feldspar bands, and a decrease in the vol. % of both the pure quartz bands and of the K-feldspar and plagioclase porphyroclasts (compare Fig. 14a with Fig. 14b). Mineral chemical reactions of the porphyroclasts to fine-grained K-feldspar $\pm$ plagioclase $\pm$ biotite $\pm$ quartz mixtures have been observed, but are not common.

As the vol. % of the pure quartz bands decreases, there is a decrease in grain size of the pure quartz bands from $31\pm9\,\mu$m ($Sk=1.2$; $Km=1.8$) in the (proto)mylonitic rocks down to $2.3\pm0.8\,\mu$m ($Sk=1.7$; $Km=2.6$) in the ultramylonites (Fig. 13c). An electron microscopy study of the microstructures and microtextures in these very fine-grained (2.3 μm) pure quartz bands is presented in Fliervoet and White (1995). They inferred dislocation creep was the dominant deformation mechanism in these fine-grained pure quartz bands. The ultramylonite itself, is made of an extremely fine-grained (0.5 μm) mixture of quartz, K-feldspar ($Or_{92.6}$), plagioclase ($An_{21.2}$) and biotite. A more detailed TEM description of the microstructures of the fine-grained polymineralic ultramylonite is given in the next section.

Temperature estimates

The mineral assemblage within the matrix of the samples is typical for that expected from rocks of granodioritic bulk composition metamorphosed under upper-greenschist-facies conditions (Turner, 1968, fig. 7-9). The absence of garnet indicates lower temperatures compared to the abovementioned coarser-grained amphibolite-facies ultramylonite. The inferred deformation conditions are similar to those reported by Shaw and Black (1991), who inferred greenschist-facies conditions (350–500°C) in similar shear zones of the Redbank Deformed Zone.

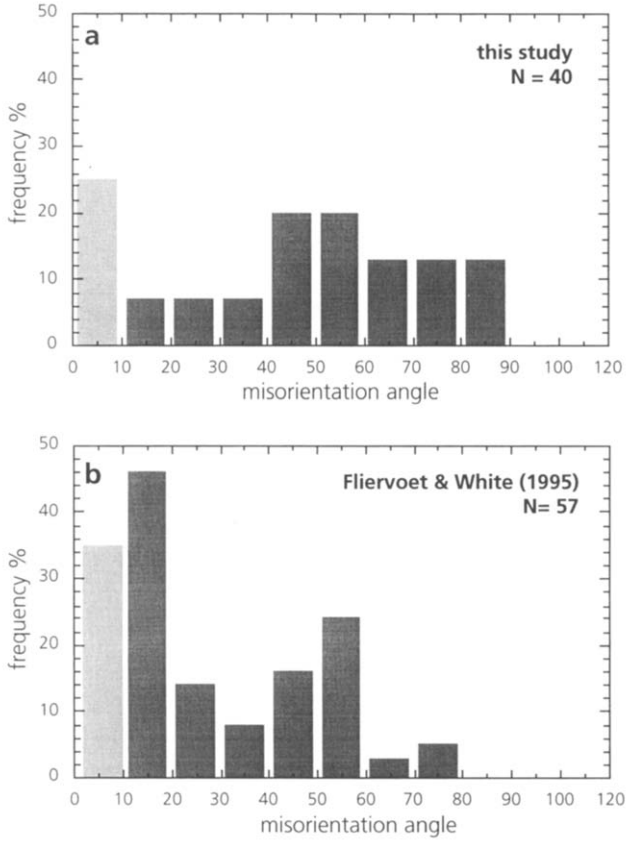

Fig. 12. Distribution of angles of misorientation between adjacent quartz grains as measured using TEM. (a) Quartz MOD in the amphibolite-facies polyphase ultramylonite; $N=40$. (b) Quartz MOD in fine-grained (2.3 μm) pure quartz bands in the greenschist-grade ultramylonite using the data of Fliervoet and White (1995). $N=57$.

TRANSMISSION ELECTRON MICROSCOPY OF THE GREENSCHIST-GRADE POLYPHASE ULTRAMYLONITE

Severe specimen charging, huge differential polishing rates and a very fine average grain size (0.5 μm) inhibited the same detailed SEM analyses as carried out for the amphibolite-facies ultramylonite. Consequently, TEM has been used to study the microstructure; examples are shown in Figs 15 & 16. Most grains could be identified using qualitative energy-dispersive spectrometry (EDS) measurements and diffraction analyses. The chemistry of some larger grains (>3 μm) have been measured using conventional microprobe methods.

The ultramylonite consists of a mixture of 35% quartz, 20% K-feldspar ($\approx Or_{94}$), 45% plagioclase ($\approx An_{21}$) and various amounts of mica (up to 20%). The grain size is small, ranging from 0.1 to 4.0 μm (median $=0.5\pm0.2$ μm; $Sk=2.5$; $Km=7.8$). The grains have a rectangular to square grain shape (Fig. 16) and are slightly elongated (sub)parallel to the foliation. Some equiaxed grains have been observed (Fig. 16).

The dislocation and defect density in all phases is generally very low. Only the larger (generally >2 μm) quartz, plagioclase and K-feldspar grains have some low angle boundaries (Fig. 15); these occur mainly perpendicular to the foliation.

Both grain and interphase boundaries show a tendency to be aligned parallel to the foliation (Fig. 15). Many of the boundaries are interlinked and are continuous across several grain diameters. The average spacing between these continuous grain boundaries is 1.7 ± 0.9 μm, equal to two–three grain diameters. This is similar (in number of grain diameters) to the spacing seen in the amphibolite-facies ultramylonites. The average length of these continuous boundaries is 2.6 ± 0.9 μm; with an average grain size of 0.5 μm there are four or five grains adjacent to a continuous grain boundary.

No voids and/or bubbles have been observed either within the grains or at the grain or interphase boundaries (Figs 15 & 16). Figure 16 shows three successive images during a ConDF experiment, the time difference between the first (Fig. 16a) and last image (Fig. 16c) was about 5 min. The boundaries always show a diffuse contrast, which widens with time. Such microstructures are interpreted to be the result of preferential beam damage of the grain and interphase boundaries. Attempts were made to resolve the structure of the grain boundaries using high-resolution electron microscopy (HREM). However, these were unsuccessful owing to too rapid irradiation damage. This rapid damage and the diffuse contrast suggest an amorphous phase at the grain and interphase boundaries.

Microtextural analyses using (micro)diffraction in TEM were also attempted. However, they were not successful owing to too rapid irradiation damage. This damage is thought to reflect a high H_2O content in the greenschist-facies ultramylonite.

DISCUSSION

Strain variations across the mylonite zones

In both the mylonite zones studied marked variations in the orientation of the foliation occur. Schematic cross-sections (amphibolite facies, Fig. 3a; greenschist facies, Fig. 13a) clearly illustrate the decreasing dip angle of the foliation within the ultramylonites (open symbols) compared to that in the (proto)mylonites (closed symbols).

As pointed out by Ramsay and Graham (1970), the intensity and orientation of the mylonitic foliation in a (simple) shear zone depends upon the magnitude of the accumulated finite strain. The systematic curvature of the foliation from the margin to the centre of the shear zone reflects an increase in accumulated finite strain. For very high shear strains, the foliation becomes subparallel to the direction of shear.

Our observations indicate that the strain in the ultramylonitic centres of both the amphibolite-facies and the greenschist-facies shear zones is higher than in the surrounding mylonites, which in turn is higher than the protomylonites. In assuming that the shear-zone

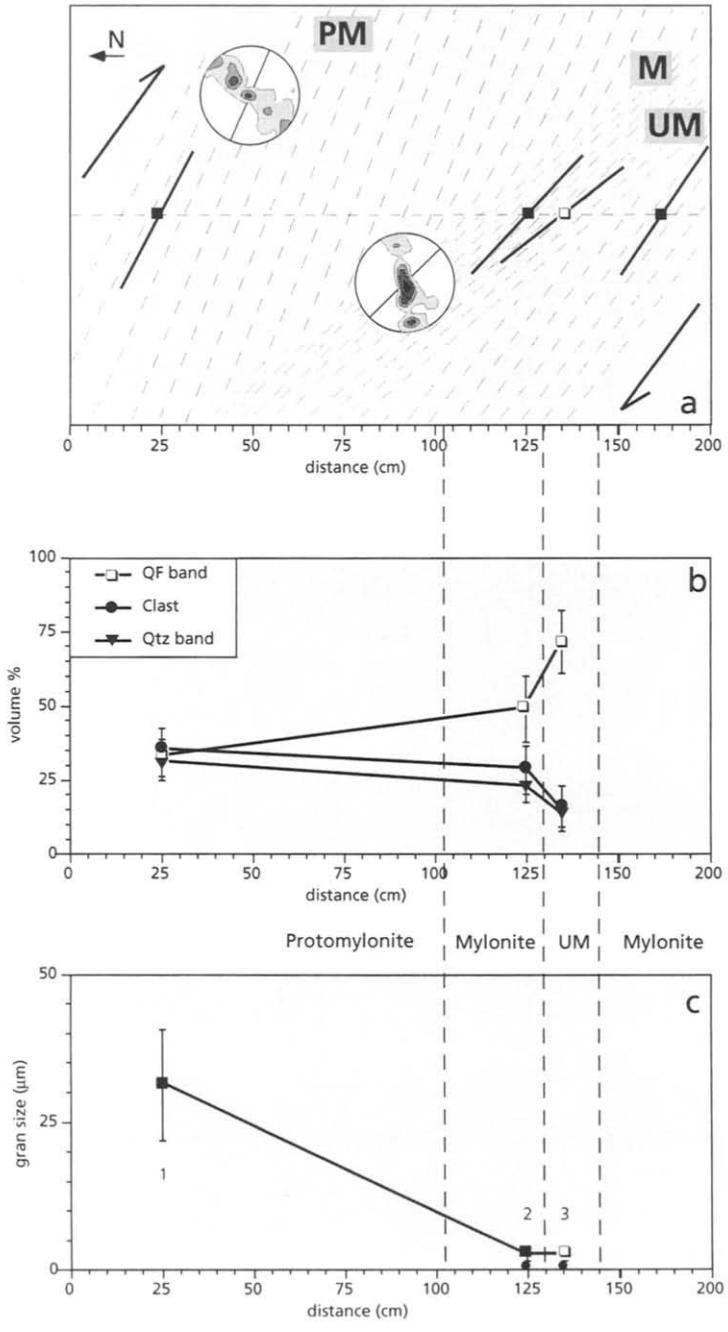

Fig. 13. Variations of microstructural features within the greenschist-facies shear zone studied. (a) Schematic cross-section showing the orientation of mylonitic foliation. Open symbols denote ultramylonitic rocks, whereas closed symbols denote encapsulating protomylonitic and mylonitic rocks. Quartz *c*-axis textures of the pure quartz bands are shown; contours drawn at 2σ; $N=190$ and $N=144$. (b) Variation of the quartz–feldspar band (QF), pure quartz band (Q) and K-feldspar and plagioclase clast (C) content. (c) Variation of the median grain size of the pure quartz bands, error bars represent half the interquartile range; the grain size of the QF bands are also indicated. UM denotes the ultramylonitic centre of the shear zone.

walls are subparallel to the foliation of the ultramylonites, the accumulated shear strains of the protomylonites and mylonites can be estimated (Ramsay and Graham, 1970). These estimates indicate shear strains of 2 in the protomylonites and of 5 in the mylonites. Shear strains accumulated within the ultramylonites must be higher.

Further evidence for higher finite strains within the ultramylonitic shear-zone centres comes from the observations on the folded pure quartz bands. The presence of such intensively 'strained' structures within the ultramylonites, and the virtual absence of these structures within the (proto)mylonites, suggests that strains were highest in the ultramylonitic centres of the shear zones. Similar observations are reported by Handy and Zingg (1991) and Stünitz and Fitz Gerald (1993). The folded to

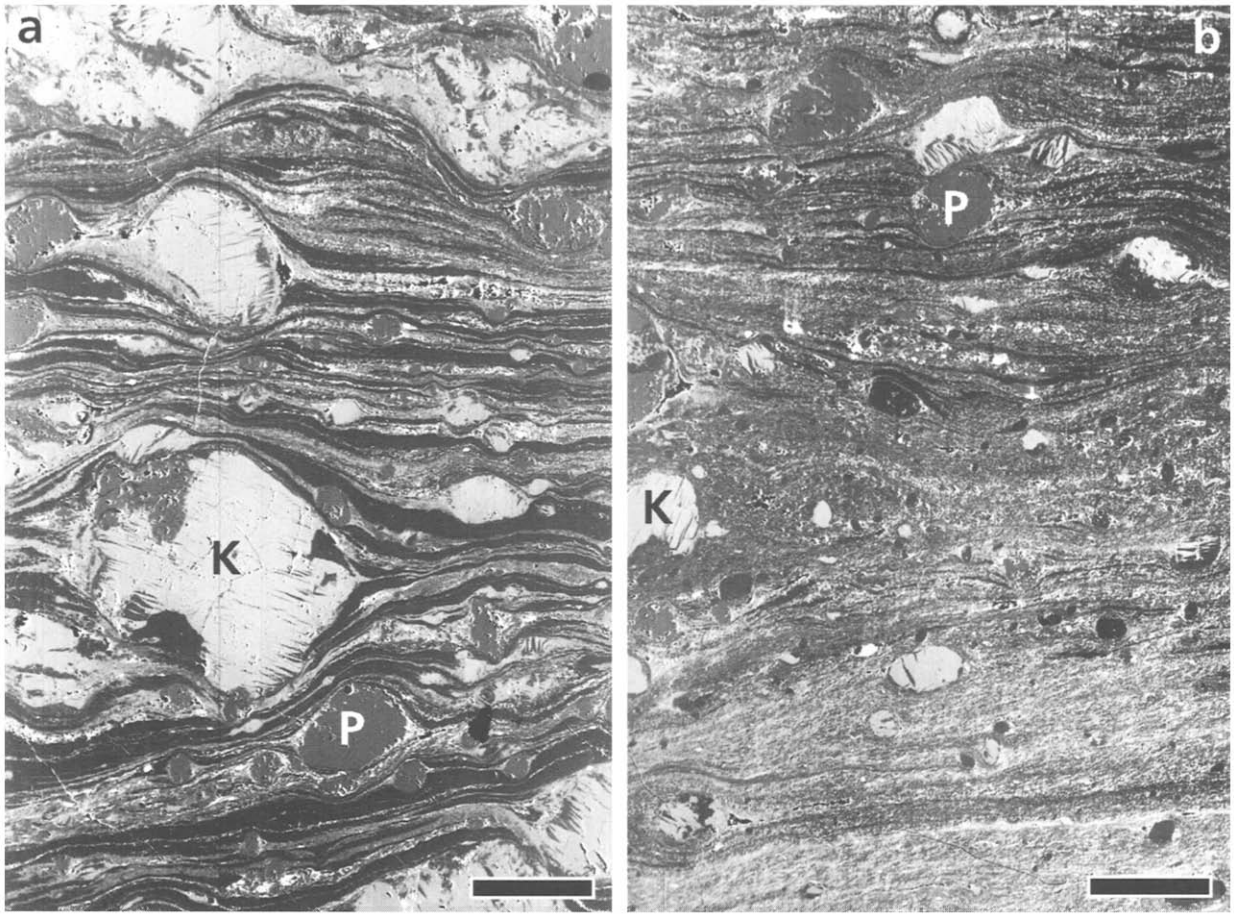

Fig. 14. SEM BSE images of microstructures in the greenschist-facies shear zone studied. (a) A typical mylonite having porphyroclasts of plagioclase (P), K-feldspar (K) and epidote embedded in a matrix of finer-grained bands of K-feldspar, plagioclase, quartz and biotite, alternating with pure quartz bands. Scale bar: 300 μm. (b) A typical ultramylonite having few porphyroclasts of K-feldspar, plagioclase embedded in a fine-grained (0.5 μm) homogeneous polyphase matrix. Note the decrease in the number of both the K-feldspar and plagioclase clasts, and the increase in percentage of quartz–feldspar bands in the ultramylonite. Scale bar: 300 μm.

unfolded ratio of 0.5 reported above, when combined with the virtual absence of folds in the mylonitic rocks, indicates that strains in the ultramylonites were at least twice as high in the ultramylonites compared to the surrounding mylonitic rocks.

In assuming that the studied shear zones narrow with time, we can use the observed progressive deformation from protomylonite to mylonite to ultramylonite as a record of history (Means, 1995). The higher strains recorded in the polyphase ultramylonitic shear-zone centre can be regarded as reflecting viscosity differences between ultramylonites and the protomylonites and mylonites (Watts and Williams, 1979; Handy and Zingg, 1991; Fitz Gerald and Stünitz, 1993). The ultramylonites are softer and have a lower viscosity, than the surrounding (proto)mylonitic rocks, i.e. higher strain rates at the same stress level. It follows that the mechanical properties of the fine-grained polyphase ultramylonites must have controlled the rheology of these high strain shear zones.

Deformation mechanisms within the ultramylonites

Microstructural criteria commonly used to infer grain-boundary sliding in such polyphase fine-grained rocks include (see also the discussion in Fliervoet, 1995; Fliervoet and White, 1995): (i) a diamond or rectangular grain shape (White, 1977; Drury and Humphreys, 1988; Stünitz and Fitz Gerald, 1993); (ii) a continuous alignment of grain and interphase boundaries over several grain diameters (White, 1977; Stünitz and Fitz Gerald, 1993; Zelin *et al.*, 1994); (iii) grain and interphase boundaries decorated with (asymmetric) voids (Gifkins, 1976; White, 1977, 1979; White and White, 1981; Behrmann, 1985); (iv) a grain size comparable to or smaller than the equilibrium subgrain size (White, 1977, 1979); and (v) aspects of any CPO generated should be weak (White, 1979; Padmanabhan and Davies, 1980; Behrmann, 1985; Rutter *et al.*, 1994). All of these microstructural and microtextural criteria are met in both fine-grained polyphase ultramylonites. It is there-

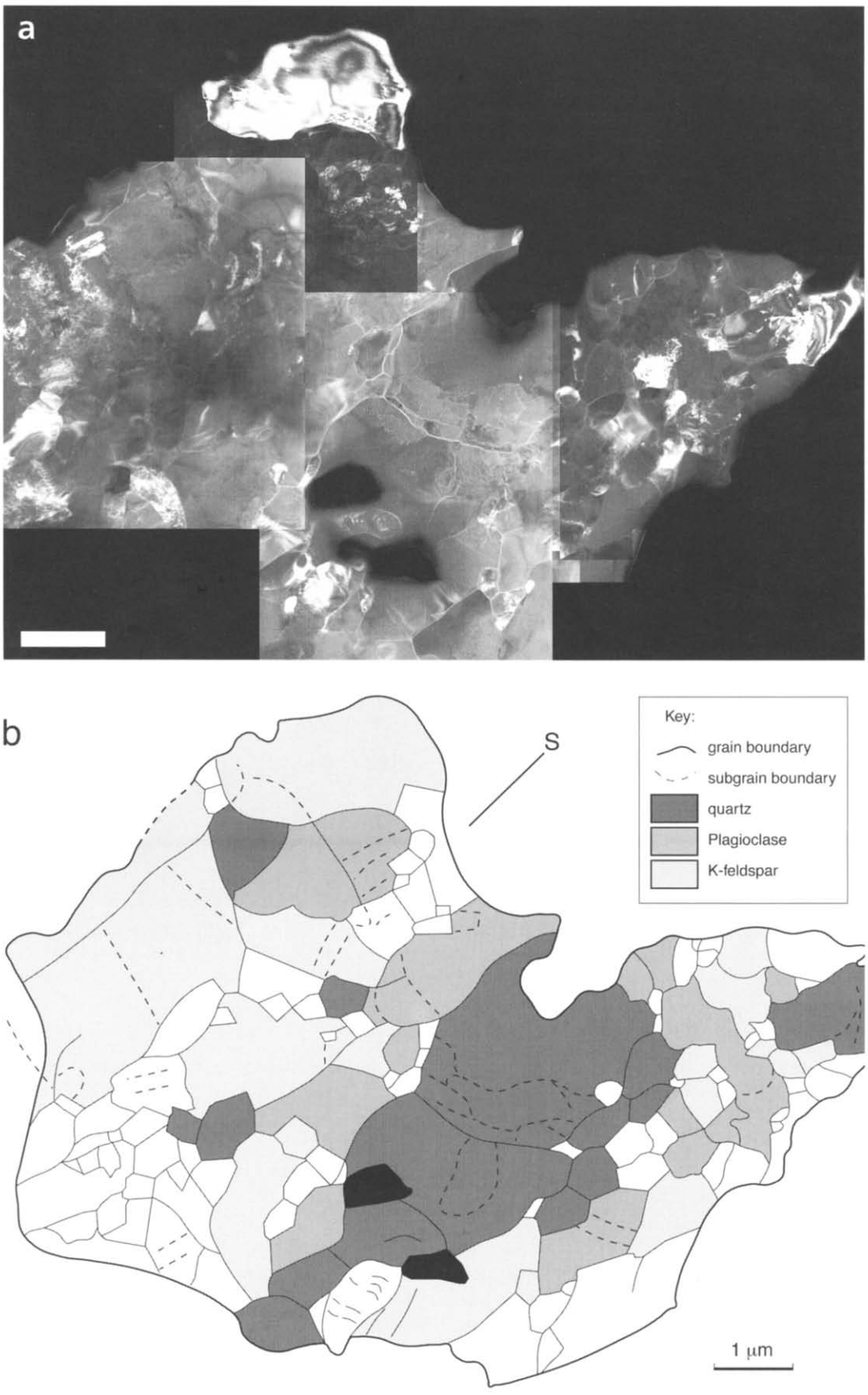

Fig. 15. (a) TEM ConDF image showing the microstructure of the greenschist-facies polyphase ultramylonite. (b) Line drawing after (a) showing the mineral distribution, and the grain and subgrain boundaries. Note the continuous alignment of grain and interphase boundaries, parallel to the foliation (marked S) across several grain diameters. The larger quartz and K-feldspar grains contain irregular subgrain boundaries.

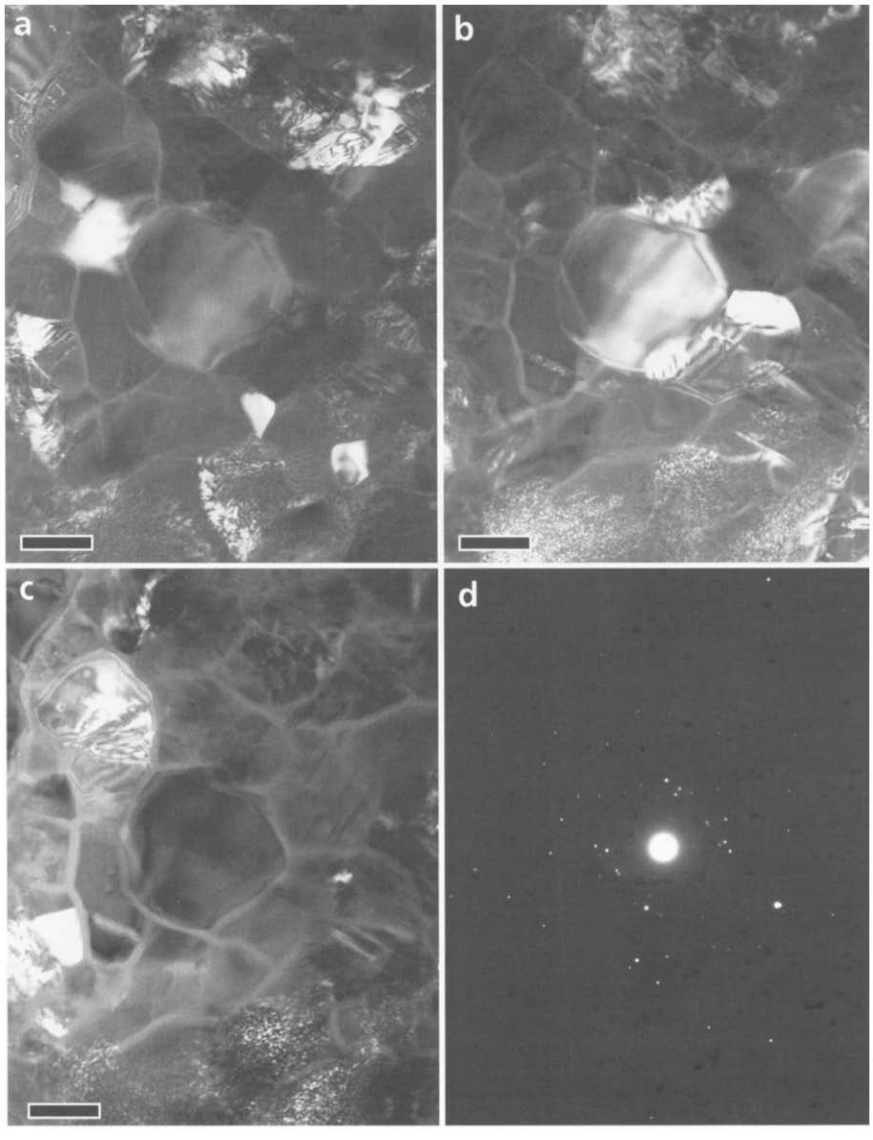

Fig. 16. (a)–(c) ConDF TEM images showing preferential electron irradiation damage of interfacial boundaries in greenschist-facies ultramylonite. With time the contrast from the boundary widens; the time difference between the first (a) and last image (c) was about 5 min. No voids and/or bubbles have been observed either within the grains or at the grain or interphase boundaries. Scale bars are 0.2 μm. (d) Diffraction pattern of the area.

fore concluded that deformation included a major component of grain-boundary sliding.

Furthermore, microtexture analyses on the quartz of the amphibolite-grade ultramylonites revealed not only a weak CPO but also no crystallographic relation between adjacent grains, in terms of the axis–angle of finite misorientation or low (<49) Σ values. Such crystallographic relationships between adjacent crystals would be expected if internal dislocation processes contributed significantly to the deformation process (see also the discussion in Beeré, 1978; Haruna *et al.*, 1992; Fliervoet, 1995; Fliervoet and White, 1995).

We have measured the texture and misorientation relationships in fine-grained (2.3 μm) pure quartz bands in the greenschist-facies ultramylonite (for details see Fliervoet, 1995; Fliervoet and White, 1995). Based on microstructural and microtextural data we argued that the dominant deformation mechanism was dislocation creep. The pertinent observations were the sharp texture, subgrain formation and recrystallization microstructures. Furthermore, the misorientation relations between adjacent grains were found to be perpendicular to the Burger's vectors known for quartz, and up to 80% of the boundaries could be described as having low Σ values. The misorientations can be explained by dislocation processes being operative.

The distribution of the angles of misorientation between adjacent quartz grains in these fine-grained pure quartz bands (Fig. 12b) is very different to the one measured between the quartz grains in the polyphase amphibolite-facies ultramylonite (Fig. 12a). The former shows numerous grain boundaries having low to intermediate misorientation angles, whereas in the latter the distribution is more uniform. Moreover, in the latter, the

axes of misorientation between adjacent quartz grains do not show any preferred orientation. As discussed by Fliervoet and White (1995), Frank's formula can be applied to quartz to elucidate the active slip systems. As the axes of misorientation between adjacent quartz grains in the amphibolite-grade ultramylonite are not perpendicular to any of the known Burger's vectors for quartz, it is suggested that dislocation activity cannot solely account for the misorientation between adjacent grains. Therefore, they are interpreted to be the result of grain rotations due to grain-boundary sliding and neighbour switching events.

Many minerals are unstable under an electron beam and transform to an amorphous phase. The rate at which this happens is a function of a number of variables such as beam intensity, beam current, accelerating voltage, temperature and impurity content. These variables have been discussed by McLaren (1991, pp. 268–283). It is generally observed that for quartz, the beam damage rate increases with water content, although some exceptions are reported (see McLaren, 1991). In this respect, the preferential irradiation damage of the interfacial boundaries of the greenschist-facies ultramylonite samples is interpreted to be the result of water present in a grain-boundary amorphous film. The increase in damage rate of the quartz grains in the greenschist-grade ultramylonite compared to those in the amphibolite-facies sample prevented microtextural analyses. It is suggested to reflect a higher H_2O content in the lower metamorphic grade ultramylonite. White and Knipe (1978) suggested that fluids can weaken grain boundaries, and therefore may facilitate grain-boundary sliding.

Mechanisms accommodating grain-boundary sliding

Grain-boundary sliding deformation cannot occur without some accompanying deformation within the grains itself (Mukherjee, 1971; Gifkins, 1976; Padmanabhan and Davies, 1980; Langdon, 1995). The grains change their shapes only as necessary to maintain continuity during creep if no fracturing occurs. In general, grain-boundary sliding is the faster process, so the rates of accommodation control the overall strain rate (Gifkins, 1976).

The observations of the intracrystalline defect structures within the amphibolite-facies ultramylonite suggest that different processes were operative within the different minerals during deformation. The quartz defect structures indicate that dislocation motion occurred within the quartz during deformation. Whether the dislocations are directly related to an accommodation mechanism or they are produced by parallel dislocation creep is difficult to assess. In fact, one can question whether these processes are distinguishable. However, their presence indicates that dislocation (glide) activity occurred. The observation that high dislocation densities are associated with high bubble densities suggest that the dislocations are bound in their glide planes by these bubbles (White, 1973; White and Knipe, 1978).

No dislocations or twins have been observed within plagioclase grains, while some evidence for twinning but no dislocations were found within the K-feldspar. No microcracks have been observed. This suggests that diffusional processes have accommodated the deformation within the plagioclase and K-feldspar. Curved interphase boundaries, such as those presented in Fig. 10(c) between K-feldspar and quartz, are generally taken as evidence for moving (interphase) boundaries (e.g. Gower and Simpson, 1992; Stünitz and Fitz Gerald, 1993). Migration of such a boundary between two dissimilar phases involves a flux of atoms, hence diffusion (K, Al and Si in the case of Fig. 10c) to and from the moving interphase boundary.

The accommodating deformation mechanisms within the greenschist-facies ultramylonite are difficult to determine. The observation that all phases were defect-free except for the larger grains ($>2\ \mu m$), and that only minor twinning has been observed, suggests that accommodation involved diffusive mass transfer.

The similar grain shapes (in terms of circularity, elongation and grain shape factor) of the plagioclase, K-feldspar and the quartz in the amphibolite-facies ultramylonite suggest that the fine-grained phases were equally deformable at the ambient conditions (pressure, temperature, chemical environment). Similar observations are reported by Stünitz and Fitz Gerald (1993), who analysed grain size and grain shape distributions in several fine-grained polyphase ultramylonites deformed at low-greenschist-facies conditions; the ultramylonites are composed of a mixture of albite, quartz and epidote. They observed no preferred curvature of the quartz–albite interphase boundaries: bulging was directed towards both quartz and albite.

The grain size of the pure quartz bands within the ultramylonitic centre of the amphibolite-facies mylonite zone is much larger ($60\ \mu m$) than the grain size of the quartz within the polyphase quartz–feldspar bands ($11 \pm 4\ \mu m$), suggesting that the latter grain size is in disequilibrium. As numerous quartz–quartz grain boundaries occur within the polyphase mixture, the question arises as to what mechanism kept the grain size below the equilibrium grain size. As no mica grains were found at the grain boundaries, the usually invoked mechanism of small mica grains pinning the grain boundary is not appropriate in this instance. Voids and bubbles on grain boundaries can inhibit grain boundaries from migrating (Rödel and Glaeser, 1990), and their presence is invoked as a possible contributory cause of the pinning. Another possible cause is the orientation of the boundaries themselves. It has been observed in metals (e.g. Gordon and Vandermeer, 1966) that the rate of grain-boundary migration depends on the misorientation between the adjacent grains. Experiments on lead bicrystals (Gordon and Vandermeer, 1966) show that grain-boundary migration rates are lower at random

boundaries compared to special, low Σ, boundaries. The misorientation relations between the quartz grains cannot be described as having low Σ relations. If the grain-boundary migration relations of quartz are similar to that of lead, this might be a cause for the small, disequilibrium, quartz grain size.

The grain size of the plagioclase and K-feldspar grains in the polyphase ultramylonite is similar to that of small domains of plagioclase or K-feldspar alone. These observations indicate that the plagioclase and K-feldspar grain sizes are stable. Similar observations have been reported by Stünitz and Fitz Gerald (1993) on fine-grained albite–quartz–epidote mixtures. It is therefore concluded that the three-dimensional dispersion of the plagioclase, K-feldspar and biotite, together with slow grain-boundary migration rates and possible inhibition of migration by bubbles and voids, inhibits the grain growth of quartz in the polyphase ultramylonites to 11 μm compared to the 60 μm of the pure quartz bands.

Progressive mylonitization

The progressive change from protomylonite to mylonite to ultramylonite, observed with increasing strain in the two shear zones studied, clearly involved a reduction in the size and in the number of K-feldspar and plagioclase porphyroclasts, a decrease in vol. % of pure quartz bands and a concomitant increase in the volume of the fine-grained polyphase mixture made up of K-feldspar, plagioclase, quartz and biotite. Concurrently, the overall grain size of the amphibolite-facies shear zone is reduced to 5–11 μm (i.e. the grain size of the polymineralic ultramylonite), whereas the overall grain size of the greenschist-facies shear zone grain size is reduced to 0.5 μm.

The question arises as to what processes have led to the formation of the polyphase quartzo-feldspathic ultramylonites in the two mylonite zones. The formation of the polyphase quartz–feldspar bands may be due either to the mechanical breakdown (recrystallization) of the porphyroclasts and/or to chemical reactions. In the case of purely mechanical breakdown, no chemical differences are expected between the porphyroclasts and the newly formed grains. Chemical reactions would produce new mineral grains stable at the ambient pressure and temperature conditions (i.e. White and Knipe, 1978; Allison *et al.*, 1979; Williams and Dixon, 1982; Dixon and Williams, 1983; Janecke and Evans, 1988; Fitz Gerald and Stünitz, 1993).

Evidence for the chemical breakdown of the K-feldspar and plagioclase clasts has been observed. The commonly observed retrograde reaction of K-feldspar to form muscovite has not been observed in either type of mylonite zone (e.g. Williams and Dixon, 1982; Dixon and Williams, 1983; Knipe and Wintsch, 1985). The clasts become a fine-grained mixture of K-feldspar ± plagioclase + quartz + biotite. The reaction is complex. As the mineral chemistries of the K-feldspar and plagioclase porphyroclasts are not dissimilar to the composition of the K-feldspar and plagioclase in the quartz–feldspar bands, chemical reactions are not the only processes involved. While pure quartz bands occur within the mylonites, they are absent in the ultramylonitic centre of the shear zone. Furthermore, in the mylonites K-feldspar and plagioclase porphyroclasts are embedded within quartz–feldspar bands of variable modal mineral composition; the breakdown products of the porphyroclasts are variable. The ultramylonitic shear-zone centre, on the other hand, is an homogeneous mixture of all phases indicating that mechanical mixing of all phases did occur. This supports the previously drawn conclusion that the ultramylonites deformed by grain-boundary sliding processes.

Implications for rheological modelling

From the above it is concluded that the main softening mechanism of both the greenschist- and the amphibolite-facies ultramylonites was due to the onset of grain-boundary sliding deformation due to the fine grain size resulting from the combined processes of recrystallization, neo-mineralization and mechanical mixing. The three-dimensional dispersion of the phases, together with unfavourable grain misorientations and the presence of voids and bubbles on grain boundaries, inhibited the grains in the polyphase mixture from growing. In the encapsulating mylonites, in contrast, quartz forms the load-bearing framework and deformed by dislocation-creep processes (see also Fliervoet, 1995; Fliervoet and White, 1995). As the strain (rate) was partitioned into the ultramylonites, they must have been weaker than the mylonites and protomylonites. Therefore, the strength of the polyphase ultramylonites controlled the rheology of the high strain bands.

This has important implications for rheological studies of the middle crust. Most models describing the rheology of quartzo-feldspathic shear zones are based on flow laws for single phase quartz deforming by dislocation-creep processes (White and Bretan, 1985; Ord and Hobbs, 1989). Our results indicate that once polyphase ultramylonite zones develop in the quartzo-feldspathic middle crust, the subsequent deformation is concentrated in them and not in the pure quartz bands or in the bands in which quartz forms the load-supporting framework. Consequently, in such circumstances, a quartz-based rheology is inappropriate. Our results indicate that a quartz-based rheology will lead to an overestimation of the strength of a middle crust in which polyphase ultramylonitic zones occur.

CONCLUSIONS

(1) SEM and TEM studies of samples from two mylonite zones (one deformed at amphibolite-facies and

one at greenschist-facies conditions) in a transcrustal shear zone (Redbank Deformed Zone of Central Australia) show that, with increasing strain, the constituent rock type changes from protomylonite to ultramylonite. The mylonite consists of porphyroclasts embedded in a matrix of alternating quartz and quartz–feldspar bands. The ultramylonites are made up of a fine-grained homogeneous polyphase mixture of K-feldspar, plagioclase, quartz and biotite.

(2) The microstructure of both the polyphase ultramylonites suggests that grain-boundary sliding processes were the dominant operative deformation mechanisms. Analyses of the CPO and misorientation between adjacent quartz grains within the amphibolite-facies polyphase ultramylonite support that dislocation activity cannot solely account for the misorientation between adjacent grains, and that it has resulted from grain rotations due to grain-boundary sliding and neighbour switching events. The pure quartz bands in the encapsulating mylonites deformed by dislocation-creep processes.

(3) Within the amphibolite-grade ultramylonite different accommodating processes were operative within the different minerals. Dislocation processes were important within quartz, while diffusion-accommodated grain-boundary sliding occurred within K-feldspar and plagioclase. The accommodating mechanisms within the greenschist-grade ultramylonite are difficult to assess, it is suggested that diffusional processes accommodated the grain-boundary sliding.

(4) The bulk strain (rate) was largely accommodated in the polyphase ultramylonitic centres of the mylonite zones. Softening of the studied mylonite zones was due to the onset of grain-boundary sliding deformation due to the fine grain size resulting from the combined processes of recrystallization, neo-mineralization and mechanical mixing, producing an ultramylonite with a small grain size deforming by grain-boundary sliding processes. A three-dimensional dispersion of the phases, together with unfavourable misorientations and grain-boundary bubbles and voids, inhibited the grains in the polyphase mixture from growing.

(5) The rheology of these mylonitic zones cannot be approximated by assuming a quartz rheology as the pure quartz bands accommodated less strain than did the polyphase ultramylonite bands. Consequently, it is concluded that the use of a pure quartz rheology has limited applicability in deformation and modelling studies of a crust containing transcrustal shear zones.

Acknowledgements—We would like to thank C. ten Brink, R. de Kloe, P. O'Brien, D. R. Rubie, R. L. M. Vissers and D. van der Wal for their help, critical review and fruitful discussions. The Journal referees, J. H. Behrmann and D. J. Prior, are thanked for their detailed comments on the manuscript. T. F. Fliervoet wishes to thank P. van Maurik for his help with the electron microscopy. A. Rekko, D. Young, T. Madigan, R. Shaw and the people from the NTGS are kindly thanked for their help and logistical support during fieldwork. This work is funded by The Netherlands Organization for Scientific Research (NWO) and was conducted under the programme of the Dutch national research school, the Venig Meinesz Research School of Geodynamics.

REFERENCES

Allison, I., Barnett, R. L. and Kerrich, R. (1979) Superplastic flow and changes in crystal chemistry of feldspars. *Tectonophysics* **53**, T41–T46.

Avé Lallement, H. G. (1985) Subgrain rotation and dynamic recrystallization of olivine, upper mantle diapirism, and extension of the Basin-and-Range province. *Tectonophysics* **119**, 89–117.

Beeré, W. (1978) Stresses and deformation at grain boundaries. *Philosophical Transactions of the Royal Society of London* **A288**, 177–196.

Behrmann, J. H. (1985) Crystal plasticity and superplasticity in quartzite: a natural example. *Tectonophysics* **115**, 101–129.

Behrmann, J. H. and Mainprice, D. (1987) Deformation mechanisms in a high-temperature quartz–feldspar mylonite: evidence for superplastic flow in the lower continental crust. *Tectonophysics* **140**, 297–305.

Black, L. P. and Shaw, R. D. (1992) U–Pb zircon chronology of prograde Proterozoic events in the Central and Southern Provinces of the Arunta Block, central Australia. *Australian Journal of Earth Sciences* **39**, 153–171.

Davis, J. C. (1986) *Statistics and Data Analysis in Geology*. John Wiley & Sons, New York.

Dixon, J. and Williams, G. (1983) Reaction softening in mylonites from the Arnaboll thrust, Sutherland. *Scottish Journal of Geology* **19**, 157–168.

Drury, M. R. and Humphreys, F. J. (1988) Microstructural shear criteria associated with grain-boundary sliding during ductile deformation. *Journal of Structural Geology* **10**, 83–89.

Edington, J. W. (1974) *Monographs in Practical Electron Microscopy in Materials Science*. Philips Technical Library. Macmillan Press, London.

Fitz Gerald, J. D. and Stünitz, H. (1993) Deformation of granitoids at low metamorphic grade. I: Reactions and grain size reduction. *Tectonophysics* **221**, 269–297.

Fliervoet, T. F. (1995) Deformation mechanisms in fine grained quartzo-feldspathic mylonites. An electron microscopy study. Ph.D. thesis, Utrecht University. *Geologica Ultraiectina* **131**.

Fliervoet, T. F., van Maurik, W. A. M., Wal, D. v. d., Drury, M. R., van Roermund, H. L. M. and White, S. H. (1995) Some applications of electron back-scatter diffraction on metals and non-metals. In *Nederlandse Vereniging voor Electronen Microscopie Jaarboek, 1995*, p. 88.

Fliervoet, T. F. and White, S. H. (1995) Quartz deformation in a very fine grained quartzo-feldspathic mylonite: A lack of evidence for dominant grain boundary sliding deformation. *Journal of Structural Geology* **17**, 1095–1109.

Gifkins, R. C. (1976) Grain boundary sliding and its accommodation during creep and superplasticity. *Metallurgical Transactions* **7A**, 1225–1232.

Gilotti, J. A. (1992) The rheologically critical matrix in arkosic mylonites along the Särv thrust, Swedish Caledonides. In *Structural Geology of Fold and Thrust Belts*, eds S. Mitra and G. W. Fisher, pp. 145–160. Hopkins University Press, Baltimore.

Goldstein, J. I. (1975) Electron optics. In *Practical Scanning Electron Microscopy. Electron and Ion Microprobe Analysis*, eds J. I. Goldstein and H. Yakowitz, pp. 21–47. Plenum Press, New York.

Goleby, B. R., Shaw, R. D., Wright, C., Kennet, B. L. N. and Lambeck, K. (1989) Geophysical evidence for 'thick-skinned' crustal deformation in central Australia. *Nature* **337**, 325–330.

Gordon, P. and Vandermeer, R. A. (1966) Grain boundary migration. In *Recrystallization, Grain Growth and Textures*, eds H. Margolin, pp. 205–266. American Society of Metals, Metals Park, Ohio.

Gottstein, G. (1992) Methoden und Anwendungen der lokalen Texturcharakterisierung. *Neue Hütte* **37**, 127–141.

Gower, R. J. W. and Simpson, C. (1992) Phase boundary mobility in naturally deformed, high-grade quartzo-feldspathic rocks: evidence for diffusional creep. *Journal of Structural Geology* **14**, 301–314.

Grimmer, H. (1980) A unique description of the relative orientation of neighbouring grains. *Acta Crystallographica* **A36**, 382–389.

Grimmer, H. (1989) *Koinzidenzorientierungen von Körnern in rhomboedrischen und hexagonalen Materialien*. PSI Bericht, Wurlingen.

Haessner, F., Pospiech, J. and Sztwiertnia, K. (1983) Spatial arrange-

ment of orientations in rolled copper. *Materials Science and Engineering* **57**, 1–14.

Handy, M. R. and Zingg, A. (1991) The tectonic and rheological evolution of an attenuated cross section of the continental crust: Ivrea crustal section, southern Alps, northwestern Italy and southern Switzerland. *Bulletin of the Geological Society of America* **103**, 236–253.

Harris, K. E. and King, A. H. (1996) Conical dark-field imaging for microstructural analysis of polycrystalline thin films. *Philips Electron Optics Bulletin* **134**, 9–14.

Haruna, T., Shibayanagi, T., Hori, S. and Furushiro, N. (1992) Effect of grain boundary characters on grain boundary sliding during superplastic deformation. *Materials Transactions of the Japanese Institute of Metals* **33**, 374–379.

Heidelbach, F. K. (1994) Textures and microstructures in recrystallized rocks; a study by X-ray and electron diffraction. Ph.D. thesis, University of California.

Heinz, A. and Neumann, P. (1991) Representation of orientation and disorientation data for cubic, hexagonal, tetragonal and orthorhombic crystals. *Acta Crystallographica* **A47**, 780–789.

Janecke, S. U. and Evans, J. P. (1988) Feldspar-influenced rock rheologies *Geology* **16**, 1064–1067.

Kleemann, U. and Reinhardt, J. (1994) Garnet–biotite thermometry revisited: the effect of Al-VI and Ti in biotite. *European Journal of Mineralogy* **6**, 925–941.

Knipe, R. J. and Wintsch, R. P. (1985) Heterogeneous deformation, foliation development, and metamorphic processes in a polyphase mylonite. In *Metamorphic Reactions—Kinetics, Textures, and Deformation*, eds A. B. Thompson and D. C. Rubie, pp. 180–210, *Advances in Physical Chemistry*, Vol. 4. Springer, New York.

Langdon, T. (1995) The characteristics of superplastic-like flow in ceramics. In *Plastic Deformation of Ceramics*, ed. R. C. Bradt, pp. 251–268. Plenum Press, New York.

Lister, G. S. (1977) Crossed-girdle *c*-axis fabrics in quartzites plastically deformed by plane strain and progressive simple shear. *Tectonophysics* **35**, 51–54.

Lloyd, G. E. and Knipe, R. J. (1992) Deformation mechanisms accommodating faulting of quartzite under upper crystal conditions. *Journal of Structural Geology* **14**, 127–144.

Mainprice, D., Lloyd, G. E. and Casey, M. (1993) Individual orientation measurements in quartz polycrystals: advantages and limitations for texture and petrophysical property determinations. *Journal of Structural Geology* **15**, 1169–1187.

Marjoribanks, R. W. and Black, L. P. (1974) Geology and geochronology of the Arunta Complex north of Ormiston Gorge, Central Australia. *Journal of the Geological Society of Australia* **21**, 291–299.

McLaren, A. C. (1986) Some speculations on the nature of high-angle grain boundaries in quartz rocks. In *Mineral and Rock Deformation: Laboratory Studies, The Paterson Volume*, eds B. E. Hobbs and H. C. Heard, pp. 233–245. American Geophysical Union Geophysical Monograph **36**.

McLaren, A. C. (1991) *Transmission Electron Microscopy of Minerals and Rocks. Cambridge Topics in Mineral Physics and Chemistry*. Cambridge University Press, Cambridge.

Means, W. D. (1995) Shear zones and rock history. *Tectonophysics* **247**, 157–160.

Mukherjee, A. K. (1971) The rate controlling mechanism in superplasticity. *Materials Science and Engineering* **8**, 83–89.

Newbury, D. E. and Yakowitz, H. (1975) Contrast mechanism of special interest in materials science. In *Practical Scanning Electron Microscopy. Electron and Ion Microprobe Analysis*, eds J. I. Goldstein and H. Yakowitz, pp. 149–208. Plenum Press, New York.

Obee, H. K. and White, S. H. (1985) Faults and associated fault rocks of the Southern Arunta block, Alice Springs Central Australia. *Journal of Structural Geology* **7**, 701–712.

Obee, H. K. and White, S. H. (1986) Microstructural and fabric heterogeneities in fault rocks associated with a fundamental fault. *Proceedings of the Royal Society of London* **A317**, 99–109.

Ord, A. and Hobbs, B. E. (1989) The strength of the continental crust, detachment zones and the development of plastic instabilities. *Tectonophysics* **158**, 269–289.

Padmanabhan, K. A. and Davies, G. J. (1980) *Superplasticity. Materials Research and Engineering*. Springer, Berlin.

Passchier, C. W. and Trouw, R. A. J. (1996) *Microtectonics*. Springer, Berlin.

Prior, D. J., Trimby, P. W., Weber, U. D. and Dingley, D. J. (1996) Orientation contrast imaging of microstructures in rocks using forescatter detectors in the scanning electron microscope. *Mineralogical Magazine* **60**, 859–869.

Ramsay, J. G. and Graham, R. H. (1970) Strain variation in shear belts. *Canadian Journal of Earth Sciences* **7**, 786–813.

Randle, V. (1992) *Microtexture Determination and its Applications*. Institute of Materials, London.

Randle, V. (1993) *The Measurement of Grain Boundary Geometry. Electron Microscopy in Materials Science*. Institute of Physics, Bristol.

Rödel, J. and Glaeser, A. (1990) Pore drag and pore-boundary separation in alumina. *Journal of the American Ceramic Society* **73**, 3302–3312.

Rutter, E. H. and Brodie, K. H. (1991) Lithosphere rheology—a note of caution. *Journal of Structural Geology* **13**, 363–367.

Rutter, E. H., Casey, M. and Burlini, L. (1994) Preferred crystallographic orientation development during the plastic and superplastic flow of calcite rocks. *Journal of Structural Geology* **16**, 1431–1446.

Schmidt, N.-H. and Olesen, N. O. (1989) Computer-aided determination of crystal-lattice orientation from electron-channeling patterns in the SEM. *Canadian Mineralogist* **27**, 15–22.

Schwarzer, R. A. (1990) Measurement of local textures with transmission electron and scanning electron microscopes. *Textures and Microstructures* **13**, 15–30.

Shaw, R. D. and Black, L. P. (1991) The history and tectonic implications of the Redbank Thrust Zone, central Australia, based on structural, metamorphic and Rb–Sr isotopic evidence. *Australian Journal of Earth Sciences* **38**, 307–332.

Sibson, R. H. (1977) Fault rocks and fault mechanisms. *Journal of the Geological Society of London* **133**, 191–213.

Stünitz, H. and Fitz Gerald, J. D. (1993) Deformation of granitoids at low metamorphic grade II: Granular flow in albite-rich mylonites. *Tectonophysics* **221**, 299–324.

Turner, F. J. (1968) *Metamorphic Petrology*. McGraw-Hill, New York.

Turner, F. J. and Weiss, V. (1963) *Structural Analysis of Metamorphic Tectonites*. McGraw-Hill, New York.

Underwood, E. E. (1970) *Quantitative Stereology*. Addison-Wesley, Reading, Massachusetts.

Venables, J. A. and Harland, C. J. (1973) Electron back-scattering pattern—A new technique for obtaining crystallographic information in the scanning electron microscope. *Philosophical Magazine* **27**, 1193–1200.

Wakefield, J. (1977) Mylonitization in the Lethakane shear zone, eastern Botswana. *Journal of the Geological Society of London* **133**, 263–275.

Watts, M. J. and Williams, G. D. (1979) Fault rocks as indicators of progressive shear deformation in the Guingamp region of Brittany. *Journal of Structural Geology* **1**, 323–332.

White, J. C. and White, S. H. (1981) On the structure of grain boundaries in tectonites. *Tectonophysics* **78**, 613–628.

White, S. H. (1973) Dislocations and bubbles in vein quartz. *Nature, Physical Sciences* **243**, 11–14.

White, S.H. (1976) The effects of strain on the microstructures, fabrics, and deformation mechanisms in quartzites. *Philosophical Transactions of the Royal Society of London* **A283**, 69–86.

White, S. H. (1977) Geological significance of recovery and recrystallization processes in quartz. *Tectonophysics* **39**, 143–170.

White, S. H. (1979) Grain and sub-grain size variations across a mylonite zone. *Contributions to Mineralogy and Petrology* **70**, 193–202.

White, S. H. and Bretan, P. G. (1985) Rheological controls on the geometry of deep faults and the tectonic delamination of the continental crust. *Tectonics* **4**, 303–309.

White, S. H., Bretan, P. G. and Rutter, E. H. (1986) Fault-zone reactivation: kinematics and mechanisms. *Philosophical Transactions of the Royal Society of London* **A317**, 81–97.

White, S. H. and Knipe, R. J. (1978) Transformation- and reaction-enhanced ductility in rocks. *Journal of the Geological Society of London* **135**, 513–516.

Williams, G. and Dixon, J. (1982) Reaction and geometrical softening in granitoid mylonites. *Textures and Microstructures* **4**, 223–239.

Woodcock, N. H. (1977) Specification of fabric shapes using an eigenvalue method. *Bulletin of the Geological Society of America* **88**, 1231–1236.

Zelin, M. G., Krasilnikov, N. A., Valiev, R. Z., Grabski, M. W., Yang, H. S. and Mukherjee, A. K. (1994) On the microstructural aspects of

the nonhomogeneity of superplastic deformation at the level of grain groups. *Acta Metallurgica et Materialia* **42**, 119–126.

APPENDIX

Scanning electron microscopy (SEM) and microprobe analyses

Atomic number contrast imaging in back-scattered electron (BSE) mode was carried out on a CamScan S2 SEM operating at 15–25 kV at a working distance of 10–25 mm. The microstructural variations associated with the change from protomylonite to mylonite to ultramylonite were quantified using 10–30 SEM photographs per sample at a magnifications of from ×50 to ×100. A measurement grid was superimposed on the micrographs with grid lines perpendicular to the foliation, along which line percentages of the different microstructural elements were calculated. As shown by Underwood (1970, chap. 2), the resultant lineal fraction is equivalent to the volume fraction of the microstructural element.

Mineral chemical analyses have been performed by combined wavelength-dispersive (WDS) and energy-dispersive (EDS) spectrometry using a Jeol JXA 8600 Superprobe. The instrument operated at an acceleration voltage of 15 kV, a beam current of 10 nA and a probe size of 1 μm. For each analysis the counting time was 60 s. No corrections for ferric iron were made. Both mineral and metal standards were used for calibration.

Analysis of the size and shape of grains and subgrains

Grain and subgrain sizes of the pure quartz bands have been measured from line drawings made from a number of photographs taken at four different flat stage orientations with respect to the polarizing directions of the light microscope. To image the grain and interphase boundaries of the amphibolite-facies ultramylonite in SEM, polished sections were etched at room temperature with HF acid vapour for about 10–30 s. Grain sizes and the orientations of the traces of grain and interphase boundaries were measured from digitized line drawings of SEM back-scattered images of etched samples using the program NIH Image 1.49 (public domain). The grain diameters were determined by taking the average of the long and short axis of each grain, which was then corrected for sectioning effects using a factor of 1.2 (cf. Underwood, 1970).

Three different measures have been used to specify grain shapes, these are the circularity, elongation and a shape factor (see also Davis, 1986, pp. 342–345):

$$\text{circularity}: C = \frac{4\pi A}{p^2} \tag{A1}$$

$$\text{elongation}: E = \frac{1}{w} \tag{A2}$$

$$\text{shape factor}: SF = \frac{p_c}{p}, \tag{A3}$$

where A is the area; p is the perimeter; l and w are the long and short axis of the grain, respectively; and p_c is the perimeter of a circle having the same area as the grain. Note that a perfect circular grain has $C = E = SF = 1$.

Electron back-scatter diffraction (EBSD) in SEM

Because of the fine grain size within the ultramylonitic bands within the mylonite zones, the SEM-based EBSD technique has been used for crystallographic preferred orientation (CPO) determinations. This technique is capable of measuring the full orientation of grains with a size down to 0.5–1 μm (Venables and Harland, 1973; Gottstein, 1992; Randle, 1992). EBSD patterns were solved using structure files containing the atomic positions within the minerals (see also Schmidt and Olesen, 1989; Mainprice *et al.*, 1993). Unfortunately, for the minerals encountered in this study, structure files are only presently available for quartz, limiting EBSD analysis to this mineral.

Two types of data are produced by the EBSD analyses. The first is the microtexture, which is the CPO on a scale that is consistent with a single unit of orientation, i.e. a grain or a subgrain (cf. Randle, 1992). The measurement of the microtexture enables the determination of the misorientation relationships between two adjacent grains or subgrains. This misorientation distribution (MOD) produces the second dataset.

In addition, orientation contrast imaging (OCI) (Fig. 4d) in back-scattered electron mode is possible by mounting a 'normal' BSE detector in the forward-scattered position underneath the EBSD detector (Newbury and Yakowitz, 1975; Prior *et al.*, 1996). In the resultant image the contrast is not related to the average atomic number, but to the orientation of the grain. This technique enables the location for each orientation measurement to be determined.

EBSD analysis were carried out on a Philips XL 30 FEG SEM (see also Fliervoet *et al.*, 1995). A field emission gun permits relatively low accelerating voltages (10–15 kV), thereby reducing sample charging on the uncoated specimens (Goldstein, 1975). EBSD patterns were analysed using the Channel$^+$ software (Schmidt and Olesen, 1989). For trigonal minerals like quartz this software is, in principle, capable of identifying the inequivalent reflections (e.g. r vs z). However, it has been found that automatic indexing of quartz results in many misidentifications of these inequivalent reflections, thereby resulting in Dauphiné twinning misorientation relationships (60° rotation around the c-axis). To overcome this problem, each solution has been rotated 60° around the c-axis and compared with the original diffraction pattern. The results were stored only if a good match for the inequivalent reflections was found. The accuracy of the measurement is estimated to be less than 1° (Schwarzer, 1990).

With the knowledge of all crystallographic axes, the relationship between two adjacent grains or subgrains can be determined by means of an axis and angle of (finite) misorientation (Randle, 1992). The determination of the misorientation involves matrix multiplication (for details see Randle, 1992, 1993) for which a Microsoft Excel spreadsheet has been written.

For quartz, there are six crystallographically equivalent ways of indexing each grain and 36 ways of expressing the misorientation (Grimmer, 1980). These misorientations occur in groups of six, with members of each group having the same angle of misorientation and rotation axes which are symmetrically equivalent (see also Mainprice *et al.*, 1993; Fliervoet and White, 1995). Commonly, the axis–angle pair that gives the smallest possible rotation is chosen as the misorientation (see also Randle, 1992, 1993; Mainprice *et al.*, 1993; Fliervoet and White, 1995), and this is the approach adopted in this study. It is assumed that the accuracy in the misorientation is equal to that in the CPO, i.e. $<1°$. This in contrast to optical techniques and TEM, where the accuracy in the CPO data is 2–5°, resulting in larger errors (5–20°) in the measured axis–angle pair of misorientation (see Avé Lallement, 1985; Fliervoet and White, 1995). For small misorientations the error in the orientation of the rotation axis can be large ($>10°$; Fliervoet and White, 1995).

To evaluate the strength and the shape of the measured textures, the eigenvalue method of Woodcock (1977) has been used. The eigenvalues have been calculated using the program Stereonet 4.9.6 (R. W. Allmendinger, public domain). The shape of a texture is defined by:

$$K = \frac{\ln(S_1/S_2)}{\ln(S_2/S_3)} \tag{A4}$$

where $S_{1\ldots3}$ are the normalized eigenvalues. Girdle distributions have $0 \leq K < 1$, whereas clustered maxima have $K \geq 1$. The strength of a texture is defined by:

$$C = \ln(S_1/S_2) \tag{A5}$$

Uniform or random distributions will have a $C \approx 0$, strong textures have a larger C. The method assumes that the textures are unimodal clusters, axially symmetric girdles or some combination of the two with (near) orthorhombic symmetry (Woodcock, 1977).

Microstructural analysis by TEM

TEM analyses were carried out on a Philips CM20 operating at 200 kV, with an EDAX DX4 analytical EDS system attached to facilitate mineral identification. TEM observations in conical dark-field (ConDF) imaging mode (cf. Harris and King, 1996) proved to be a suitable technique to study the microstructure of the very fine-grained (0.5 μm) greenschist-grade samples. In this mode, dark-field (DF) images are formed by the integration of all electrons that are scattered

or diffracted under the same angle but in different directions. The incident beam is tilted to a chosen angle, as for conventional DF imaging, and then rotated around the optical axis of the microscope. For grain size determinations between six and eight images were collected at successive rotations around the optic axis. These were superimposed to make line drawings. The ConDF technique could not be used for textural analysis (cf. Harris and King, 1996) as the samples are polymineralic.

Measurements of the number of free dislocations within quartz were carried out by counting dislocation terminations with the foil. The free dislocation density is defined by the number per unit area of all linear lattice defects which appear not to be bound in subgrain walls or dislocation hedges. In the analyses a random orientation distribution of the dislocation lines was assumed (cf. Underwood, 1970). Rapid irradiation damage prevented direct characterization of dislocation Burger's vectors. Grain- and subgrain-boundary orientations were measured by tilting the boundary in a vertical position, i.e. parallel to the incident electron beam (cf. Edington, 1974); the image and the tilt angles were recorded. Errors were estimated at 5–10°. Standard trace analyses techniques were used to obtain the orientation of the boundary in crystal coordinates (see Edington, 1974). Bubbles within quartz grains were imaged in TEM using various two-beam conditions; these images were subsequently superimposed to make line drawings.

As for the grain size measured in SEM and optical microscopy, dislocation density and bubble size all show log-normal distributions (Davis, 1986). Consequently, the median of the (normal) distribution was taken as a measure of the size; half the interquartile range is taken as a measure of variability; the skewness (*Sk*) and kurtosis (*Km*) are given to characterize the spread of data around the median.

Microtextural analysis by TEM

Quartz textures were measured using TEM in fine-grained (2.3 μm) quartz bands in similar rock types. The data and analyses are presented in Fliervoet (1995) and Fliervoet and White (1995). It was concluded in these studies that the quartz bands deformed by dominant dislocation-creep processes. In the TEM study no record was made of inequivalent reflections (e.g. r vs. z), quartz being treated as having an hexagonal diffraction symmetry. To compare the two datasets, TEM was used to measure the CPO of quartz within the polyphase ultramylonite (details of the method are given in Fliervoet and White, 1995). Quartz texture analyses of the greenschist-facies polymineralic ultramylonites have been attempted by means of TEM, but were not successful because of extremely rapid beam damage. Severe specimen charging, huge differential polishing rates and a very fine average grain size (0.5 μm) inhibited the EBSD analysis in SEM. EBSD analysis of the fine-grained (2.3 μm) pure quartz bands was not successful due to very poor EBSD pattern quality.